Extracting Shape and Reflectance of Lambertian, Specular, and Hybrid Surfaces

Shree K. Nayar, Katsushi Ikeuchi, and Takeo Kanade

CMU-RI-TR-88-14

The Robotics Institute
Carnegie Mellon University
Pittsburgh, Pennsylvania 15213

August 1988

This work was supported by the Westinghouse Electric Corporation. K. Ikeuchi and T. Kanade are supported in part by DARPA under Contract F33615-87-C-1499.

1 Introduction

For a given illumination, the brightness or intensity distribution in the image of an object is related to its surface shape. The first efforts in determining the shape of an object from image intensities were made by Horn [4]. More popularly known as "shape from shading," his method attempts to determine object shape from a single image of the object by studying the variation of intensities in the image. Horn formulated the problem as a first order partial differential equation and proposed a solution to the equation by using the characteristic strip expansion method. By starting with a seed point of known orientation, the orientations of points may be computed along strips that originate from the seed point. The reliability of the approach greatly depends on the selection of the starting point. Later, Ikeuchi and Horn [9] developed a shape from shading technique that uses the occluding boundaries of the object and surface smoothness constraints to iteratively compute surface orientations from image intensities. Both the above methods are *global* in that they compute orientations by propagating previously computed orientation information. The first *local* approach to shape from shading was presented by Pentland [14]; it assumes that every small region in the image lies on a spherical surface. The intensity variations inside a region are used to find the sphere that region represents. Local orientation is computed by finding the location of the region on its corresponding sphere. All shape from shading methods make assumptions (usually Lambertian) regarding the surface reflection model to compute orientations. However, even if the surface reflectance model is accurately known, it is not possible to find a unique surface orientation from a single image intensity value without using additional shape constraints. For this reason, shape from shading methods lack the generality that is desired in a shape extraction technique.

The number of possible orientations that a surface point can have is considerably reduced if multiple images of the object are used where each image corresponds to a different illumination direction. Hence, several shape extraction methods are based on *actively* controlled object illumination. Woodham [21] proposed the theory for the photometric stereo method that illuminates the object from three different source directions and captures an image of the object for each source direction. The object position and the viewing direction of the camera are kept unchanged while the source direction is varied. The image intensities recorded at each surface point uniquely determine the orientation of the surface point. This mapping of intensities to orientations is possible only if the reflectance properties of the surface are known a-priori. Silver [18] developed ways to apply the basic photometric stereo method to surfaces of differing reflectance properties. Ikeuchi [11] used photometric stereo to measure orientations of a specular surface by illuminating the surface with extended light sources. Nayar and Sanderson [13] extended Ikeuchi's method by using complementary line sources to extract the shape of specular surfaces. All techniques that are developed on the

basis of photometric stereo require knowledge about the surface reflectance properties.

In recent years, the importance of understanding and using specular reflections has been realized, and considerable effort is being directed in this area. Klinker, Shafer, and Kanade [12] have succeeded in using physical models to separate specular highlights from color images of objects. Healey and Binford [3] have described ways of inferring local second order surface shape by examining the image intensities in the area of the specular highlight. Their system is also capable of predicting the appearances of specular highlights from surface models, a feature that may be used in computer graphics applications. Sanderson, Weiss, and Nayar [17] have implemented the structured highlight inspection system that determines the shape of specular surfaces. Their method is based on active sensing; an array of point sources, positioned around the object, is scanned, and the highlights resulting from each source are used to compute local orientation information.

The above mentioned shape extraction methods rely on prior knowledge of surface reflectance properties in order to extract surface shape. In many vision applications, the reflectance properties of object surfaces are not readily available. Further, these methods are only capable of determining the shape of either Lambertian or specular surfaces. An extraction method must overcome these limitation to be applicable to a variety of industrial tasks. Coleman and Jain [2] have proposed a four-source photometric stereo method that uses an extra light source to detect and avoid specular reflections. If the surface point has Lambertian and specular components of reflection, due to high sharpness of specularity, at most one of the four point sources can generate specular reflections at that surface point. Very high image intensities are discarded as highlight or specular reflections, and the remaining Lambertian intensities are used to determine surface orientations by photometric stereo.

Although this method was developed to extract the shape of hybrid surfaces whose reflectance models include both Lambertian and specular components it can only be applied to surfaces that have a reasonably strong Lambertian component of reflection; highly specular surfaces, such as smooth metallic surfaces, do not fall under this category. In practice, it may be required to extract the shape of surfaces of varying reflectance characteristics. Therefore, it is desirable to have a method that can extract the shape of Lambertian, specular, and hybrid surfaces.

Yet another limitation of all existing extraction methods is their inability to furnish information regarding the reflectance properties of the object surface. In many industrial applications, surface polish and surface roughness are found to be important inspection criteria. In such cases, surface reflectance properties may be interpreted as measures of surface polish and roughness. Further, reflectance properties may be used to segment an image in different regions; each region may be regarded as a different surface to aid the process of inspection. For these reasons, it would be of great value to have a technique that could, in addition to

determining shape, also estimate the reflectance properties of each surface point.

This paper presents a method for determining the shape of objects whose surfaces are Lambertian, specular, or hybrid. Shape information is extracted without prior knowledge of the relative strengths of the Lambertian and specular reflection components. The method also determines the parameters of the reflectance model at each surface point. The proposed method, called photometric sampling, uses extended light sources to illuminate the object surface. A sequence of images of the object is generated by changing the extended source position. An extraction algorithm uses the image intensity values recorded at each surface point to locally estimate orientation and reflectance information. A prototype implementation of the photometric sampling method was used to conduct experiments on Lambertian, specular, and hybrid surfaces. The experimental results have shown high accuracy in extracted object shape and surface reflectance properties.

2 Photometric Sampling

The intensity distribution in the image of an object is closely related to the reflectance properties and shape of the object surface, and the characteristics of the light source used to illuminate the object. The basic photometric function[1] is defined as one that relates image intensity to surface orientation, surface reflectance, and source position for point source illumination of the surface. Point light sources are most often used to illuminate a scene of interest. However, the ease of using point sources comes with the inability to capture, in the image intensities, the information that is required to extract surface features such as shape and reflectance. We propose an extended light source illumination method to overcome the inadequacies of point source illumination. The basic photometric function is modified for object illumination using extended sources. Samples of the modified photometric function may be obtained by illuminating the surface from different source directions. In the next section, we will develop an algorithm for determining surface orientations and reflectance properties from the measured photometric samples. For ease of description, photometric sampling is described here by using a two-dimensional illumination and imaging geometry. Later, these results are extended to three dimensions.

2.1 Basic Photometric Function

Consider the illumination of an object by a point source of light, as shown in Figure 1. The point source emits light in all directions. Light energy reflected by the surface in the

[1]The photometric function is similar to the image irradiance [6] equation, since image intensity is assumed to be proportional to image irradiance.

direction of the camera causes an image of the surface to be formed in the camera. For a given orientation of the surface and direction of the point source, the amount of light energy reflected by the surface in a particular direction is determined by its reflectance properties. The reflectance model of a large number of surfaces comprises two components, namely, the Lambertian (diffuse) component and the specular (gloss) component. In general, the energy of light reflected by a surface in any direction is a combination of the Lambertian and specular components. Therefore, the intensity at an image point may be expressed as:

$$I = IL + IS, \tag{1}$$

where IL is the image intensity due to Lambertian reflection and IS is the image intensity due to specular reflection.

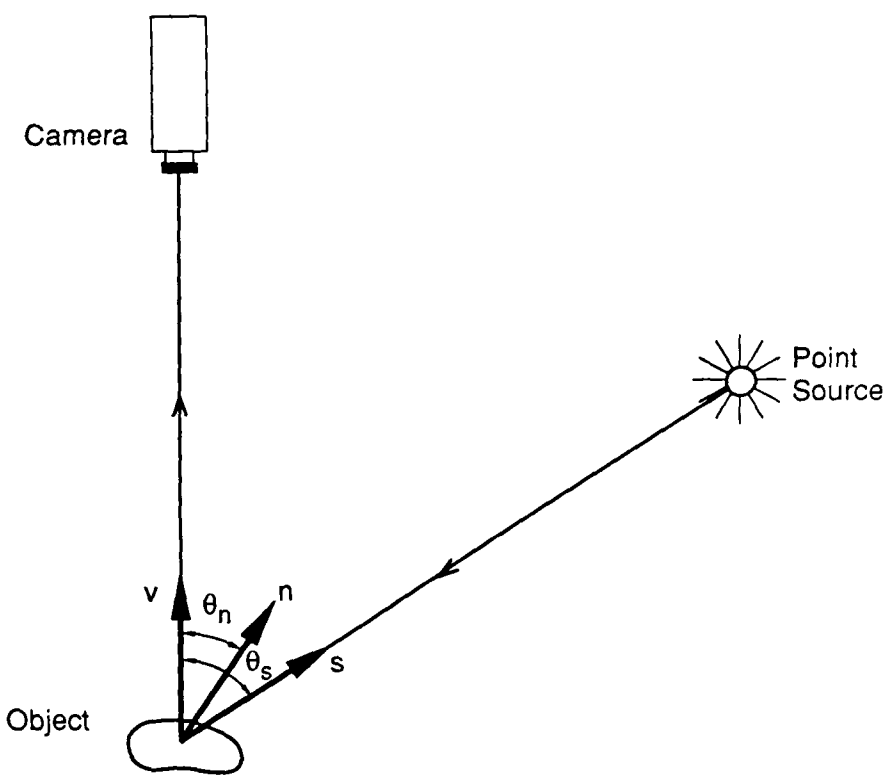

Figure 1: Two-dimensional illumination and imaging geometry. A surface element with orientation θ_n reflects light from the point source direction θ_s into the camera.

We will express the two components of image intensity in terms of the parameters that describe the two-dimensional imaging and illumination geometry shown in Figure 1. In two

dimensions, the source direction vector **s**, surface normal vector **n**, and viewing direction vector **v** lie in the same plane. Therefore, any direction may be represented by a single parameter, namely, the azimuth angle θ.

The Lambertian component IL results from the non-homogeneous nature of the layers that constitute the object surface. Light rays penetrating the surface undergo multiple refractions and reflections at the boundaries between surface layers and reemerge near the point of entry with a variety of directions. These surfaces appear equally bright from all directions; the intensity component IL is independent of the viewing direction. However, the brightness of a Lambertian surface point is proportional to the energy of incident light. As seen in Figure 1, the amount of light energy falling on the surface element is proportional to the area of the surface element as seen from the point source position, often referred to as the foreshortened area. The foreshortened area is a cosine function of the angle between the surface orientation direction θ_n and the source direction θ_s. Therefore the Lambertian intensity component IL may be written as:

$$IL = A\,cos(\theta_s - \theta_n), \tag{2}$$

where A is a constant of proportionality.

Various specular reflectance models have been developed over the years. The Torrence and Sparrow model [20] has received considerable attention in recent years as it is one of the first models derived by studying the physics underlying specular reflection. This model assumes that a surface is composed of small, randomly oriented, mirror-like facets. The specular intensities predicted by the model were in good agreement with experimental results for both metals and non-metals [20]. By using this model, the relationship between the specular intensity IS, surface orientation θ_n, and source direction θ_s may be written as:

$$IS = CFP(\eta)\frac{G}{cos\theta_n}, \tag{3}$$

where:

$$\eta = \frac{\theta_s}{2} - \theta_n.$$

The term C represents the characteristics of the light source used to illuminate the surface. The Fresnel coefficient F models the fraction of incident light that is reflected by an individual facet. The Fresnel equations predict that F is a nearly constant function of angle of incidence for materials that have a significant specular reflection component [19]. The probability distribution function $P(\eta)$ describes the orientation of the microfacets with respect to the mean surface orientation θ_n. Most often, the Gaussian distribution function is used for $P(\eta)$. The factor G quantifies the geometrical attenuation of reflected light energy due to the shadowing and masking of facets by adjacent facets.

The Torrance and Sparrow model was developed with the primary objective of describing the phenomenon of off-specular reflection from roughened surfaces. For rough surfaces, the peak in reflected intensity was observed when the angle of reflection was greater than the angle of incidence. This effect was attributed to the term $G/cos\theta_n$ in equation 3. In the experiments conducted by Torrence and Sparrow, reflected intensity was measured by varying the viewing direction while the source direction was kept constant. Therefore, for viewing directions close to the grazing angle, $cos\theta_n$ approaches zero and the reflected intensity attained very high magnitudes.

The goal of this paper is to extract surface properties by changing the source direction while keeping the viewing direction constant. Hence, for all image intensities measured at the same surface point, the term $cos\theta_n$ is constant. Further, as the source direction θ_s is varied the distribution function $P(\eta)$ changes much faster that the geometrical attenuation factor G [3]. Since $P(\eta)$ has a maximum value at $\theta_s = 2\theta_n$, the specular intensity IS is maximum when $\theta_s = 2\theta_n$. Therefore, if the source direction is varied, rather than the viewing direction, a peak in the reflected intensity is expected when the angle of reflection equals the angle of incidence.

In this paper, we focus our attention on smooth surfaces. For such surfaces, the microfacet orientation distribution may be described using a Gaussian distribution of very low variance. The resulting specular intensity IS is a very sharp function of the source direction θ_s. Therefore, the specular reflectance model given by equation 3 can be approximated by a unit impulse function:

$$IS = B\,u(\theta_s - 2\theta_n)\,, \tag{4}$$

where:

$$u(\theta_s - 2\theta_n) = \lim_{\epsilon \to \infty} \int_{\theta_s - \epsilon}^{\theta_s + \epsilon} \delta(\theta - 2\theta_n)\, d\theta = \begin{cases} 1 & \text{if } \theta_s = 2\theta_n \\ 0 & \text{otherwise} \end{cases}$$

The basic photometric function relates image intensity to surface orientation, surface reflectance, and source direction and may be written by substituting equations 2 and 4 in equation 1:

$$I = A\,cos(\theta_s - \theta_n) + B\,u(\theta_s - 2\theta_n)\,. \tag{5}$$

The constants A and B in equation 5 represent the relative strengths of the Lambertian and specular components of reflection. We see that, $A > 0$ and $B = 0$ for a purely Lambertian surface, $A = 0$ and $B > 0$ for a purely specular surface, and $A > 0$ and $B > 0$ for a hybrid surface.

Our objective is to determine orientation and reflectance at each surface point from a set of image intensities that result from changing the source direction θ_s. As seen in Figure 1, by moving the source around the object, we can vary the source direction without changing

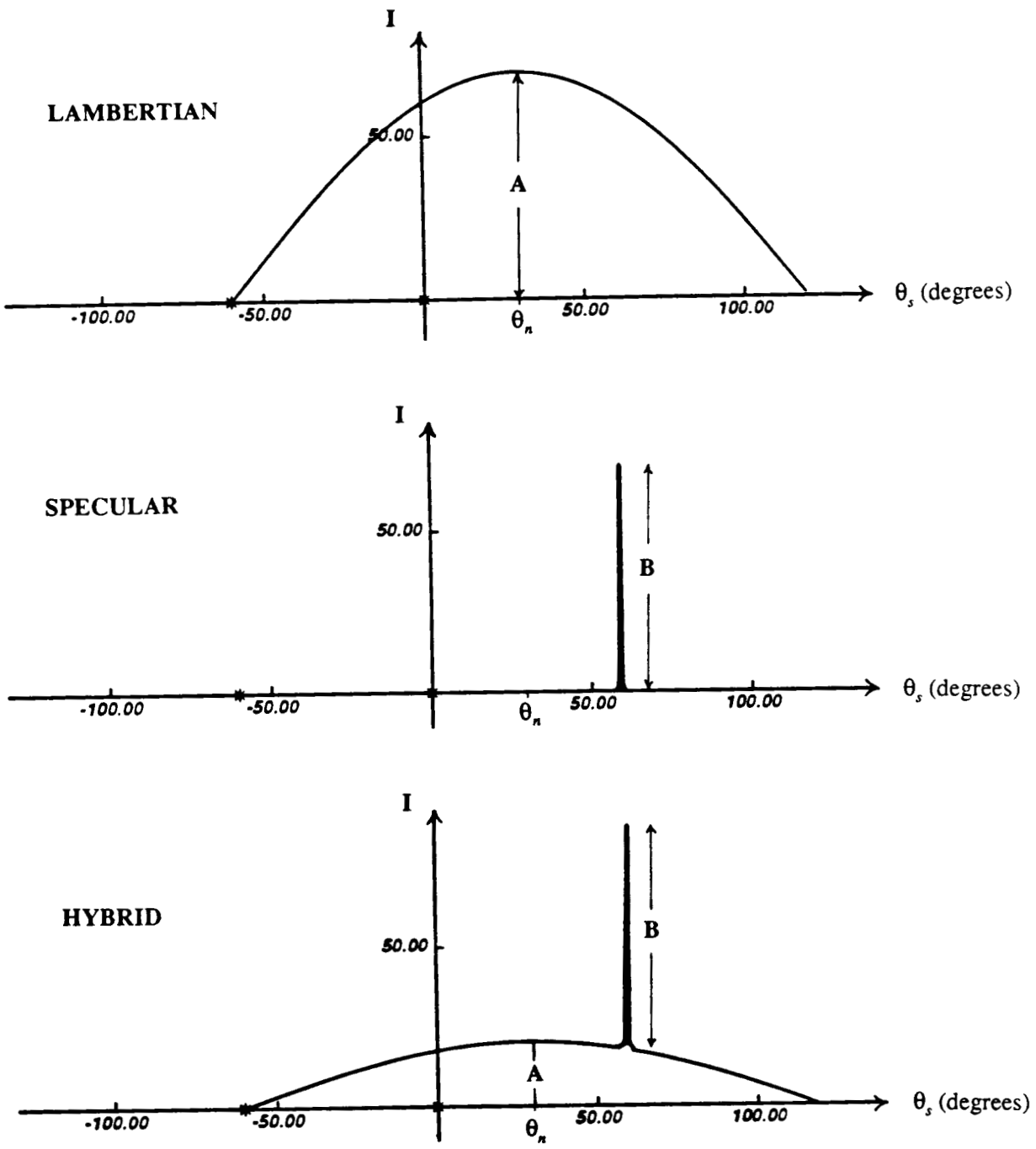

Figure 2: Basic photometric function $I(\theta_s)$ for Lambertian, specular, and hybrid surfaces.

determined by the illumination geometry and the shape of the diffuser. In order to use image intensities resulting from extended source illumination, we need to know the radiation characteristics of the extended source. The radiance function $L(\theta, \theta_s)$ for an extended source of a particular geometry is derived in Appendix A.1. The position of an extended source is determined by the direction θ_s of the point source used to generate the extended source. The radiance function $L(\theta, \theta_s)$ is symmetric with respect to $\theta = \theta_s$ and its magnitude decreases as θ deviates from θ_s. All extended sources have a width of 2α, and $L(\theta, \theta_s) = 0$ for $\theta < \theta_s$-α and $\theta > \theta_s$+α. We will refer to α as the source termination angle of an extended source. Radiance functions for both two-dimensional and three-dimensional extended source are given in Appendix A. These results will be extensively used in the following discussions.

2.3 Photometric Function for Extended Sources

The photometric function for point source illumination (equation 5) needs to be modified for extended source illumination. An extended source may be thought of as a collection of point sources where each point source has a radiant intensity that is dependent on its position on the extended source. The intensity of light reflected by an object surface that is illuminated by an extended source may be determined by computing the integral of the light energy reflected from all points on the extended source. Therefore, the modified photometric function $I'(\theta_s)$ is determined by convolving the basic photometric function $I(\theta)$ with the extended source radiance function $L(\theta, \theta_s)$. This operation is illustrated in Figure 3.

For a surface point of orientation θ_n, the Lambertian component IL' of the modified photometric function is determined as:

$$IL' = A \int_{\theta_s-\alpha}^{\theta_s+\alpha} L(\theta, \theta_s) \cos(\theta - \theta_n)\, d\theta\,. \tag{6}$$

The limits of the integral are determined by the width of the extended source (see Appendix A). In order to compute the above integral, we will use the trigonometric indentity:

$$\cos(\theta - \theta_n) = \cos\theta \cos\theta_n + \sin\theta \sin\theta_n. \tag{7}$$

Equation 6 may thus be written as:

$$\begin{aligned} IL' = {} & A \int_{\theta_s-\alpha}^{\theta_s+\alpha} L(\theta, \theta_s) \cos\theta \cos\theta_n\, d\theta \\ & + A \int_{\theta_s-\alpha}^{\theta_s+\alpha} L(\theta, \theta_s) \sin\theta \sin\theta_n\, d\theta\,. \end{aligned} \tag{8}$$

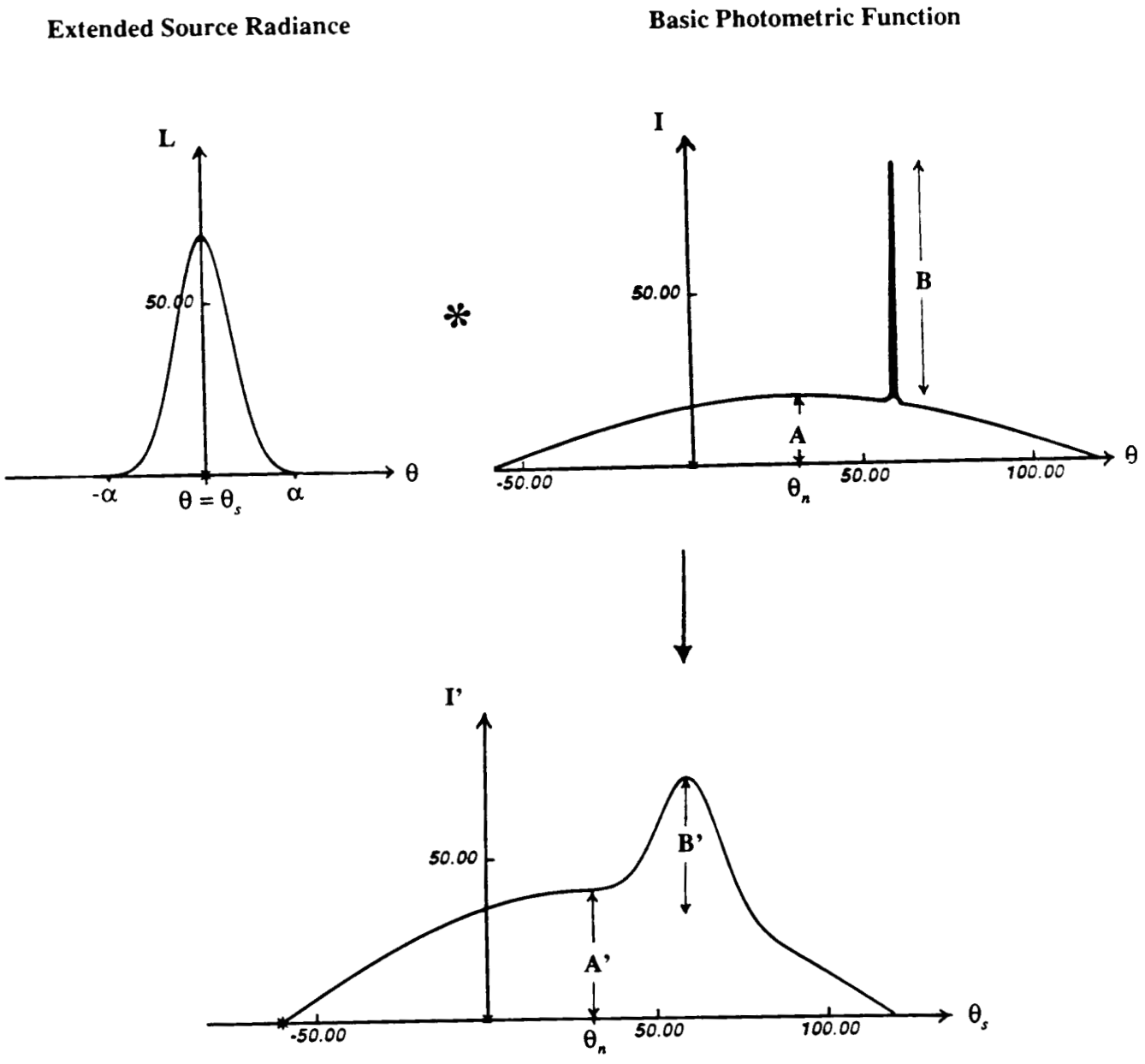

Figure 3: The photometric function for extended source illumination is obtained by convolving the basic photometric function with the extended source radiance function.

By making the substitutions:

$$cos\theta = cos(\theta - \theta_s + \theta_s) \tag{9}$$

and:

$$sin\theta = sin(\theta - \theta_s + \theta_s) \tag{10}$$

in equation 8, we obtain:

$$\begin{aligned} IL' = {} & A\, cos\theta_n cos\theta_s \int_{\theta_s-\alpha}^{\theta_s+\alpha} L(\theta,\theta_s)\, cos(\theta-\theta_s)\, d\theta \\ & - A\, cos\theta_n sin\theta_s \int_{\theta_s-\alpha}^{\theta_s+\alpha} L(\theta,\theta_s)\, sin(\theta-\theta_s)\, d\theta \\ & + A\, sin\theta_n cos\theta_s \int_{\theta_s-\alpha}^{\theta_s+\alpha} L(\theta,\theta_s)\, sin(\theta-\theta_s)\, d\theta \\ & + A\, sin\theta_n sin\theta_s \int_{\theta_s-\alpha}^{\theta_s+\alpha} L(\theta,\theta_s)\, cos(\theta-\theta_s)\, d\theta \end{aligned} \tag{11}$$

The extended source radiance $L(\theta,\theta_s)$ is an even function about the point $\theta = \theta_s$ while $sin(\theta - \theta_s)$ is an odd function about the point $\theta = \theta_s$. Therefore, the second and third integrals are equal to zero and the above equation may be simplified and written as:

$$IL' = A'\, cos(\theta_s - \theta_n), \tag{12}$$

where:

$$A' = A \int_{\theta_s-\alpha}^{\theta_s+\alpha} L(\theta,\theta_s)\, cos(\theta-\theta_s)\, d\theta\,. \tag{13}$$

Both functions $L(\theta,\theta_s)$and $cos(\theta - \theta_s)$ in equation 13 are symmetric about $\theta = \theta_s$ for all extended source directions θ_s. Thus, the value of the A' is independent of the extended source direction θ_s. It is interesting to note that the Lambertian component of the modified photometric function is only a scaled version of the Lambertian component of the basic photometric function. This result is a consequence of using an extended source whose radiance function $L(\theta,\theta_s)$ is symmetric with respect to its direction θ_s.

On similar lines, the specular intensity component IS' resulting from the extended source $L(\theta,\theta_s)$ is determined as:

$$IS' = B \int_{\theta_s-\alpha}^{\theta_s+\alpha} L(\theta,\theta_s)\, \delta(\theta - 2\theta_n)\, d\theta\,, \tag{14}$$

or:

$$IS' = B\, L(2\theta_n, \theta_s)\,. \tag{15}$$

If a more accurate specular reflection model is used [20], rather than a unit impulse function, the result of the integral would be different. However, for smooth surfaces, the specular intensity changes with the source direction θ_s much faster than the extended source radiance function $L(\theta, \theta_s)$. For such surfaces, it is reasonable to assume that the specular intensity IS' is proportional to $L(2\theta_n,\theta_s)$, while the constant of proportionality between IS' and $L(2\theta_n,\theta_s)$ varies with the parameters of the specular reflectance model used. To this end, we will use the constant B', rather than B, to represent the strength of the specular component of the photometric function. The image intensity I' at a surface point of orientation θ_n, resulting from the extended source $L(\theta, \theta_s)$, is a combination of the Lambertian component IL' and the specular component IS':

$$I' = A' cos(\theta_s - \theta_n) + B' L(2\theta_n, \theta_s). \tag{16}$$

Equation 16 is the modified photometric function that relates image intensity to surface orientation, surface reflectance, and source position for extended source illumination. In the equation, surface orientation and reflectance parameters are unknown, but constant, for a given surface point. For this reason, we will frequently refer to the modified photometric function as $I'(\theta_s)$, a relation between image intensity and extended source direction.

2.4 Sampling

The process of measuring image intensity for different source directions is equivalent to sampling the modified photometric function $I'(\theta_s)$ as shown in Figure 4. Samples of the photometric function may be obtained by moving an extended source around the object and taking images of the object for different source positions. An alternative approach would be to distribute an array of extended sources around the object such that each source illuminates the object from a different direction. The entire array of extended sources may be sequentially scanned such that for each scan a single source is active and an image of the object surface is obtained. For now we will confine the sampling process to two-dimensions; the surface normal vector, viewing direction vector, and source direction vectors for all extended sources are coplanar. Discrete extended source directions are represented by θ_i, and the photometric sample resulting from an extended source in the direction θ_i is referred to as I'_i. Therefore, the scanning process results in a set of image intensities $\{I'_i$: i=1,2,.....M$\}$ measured at each point on the object surface.

The number of samples measured at each surface point is determined by the frequency f at which $I'(\theta_s)$ is sampled. As stated earlier, in order to extract the shape and reflectance parameters of hybrid surfaces, both Lambertian and specular components of image intensity must be detected. Since we have used a unit impulse specular reflection model, the period

of the photometric function that contains specular intensities is equal to the width, 2α, of the extended source radiance function. In the following section, we will show that, in general, at least two photometric samples must have non-zero specular intensities for the extraction technique to work. Hence, the photometric function must be sampled at a frequency greater than or equal to the *minimum sampling frequency*[2] $f_{\min}$, where:

$$f_{\min} = \frac{1}{\alpha}. \tag{17}$$

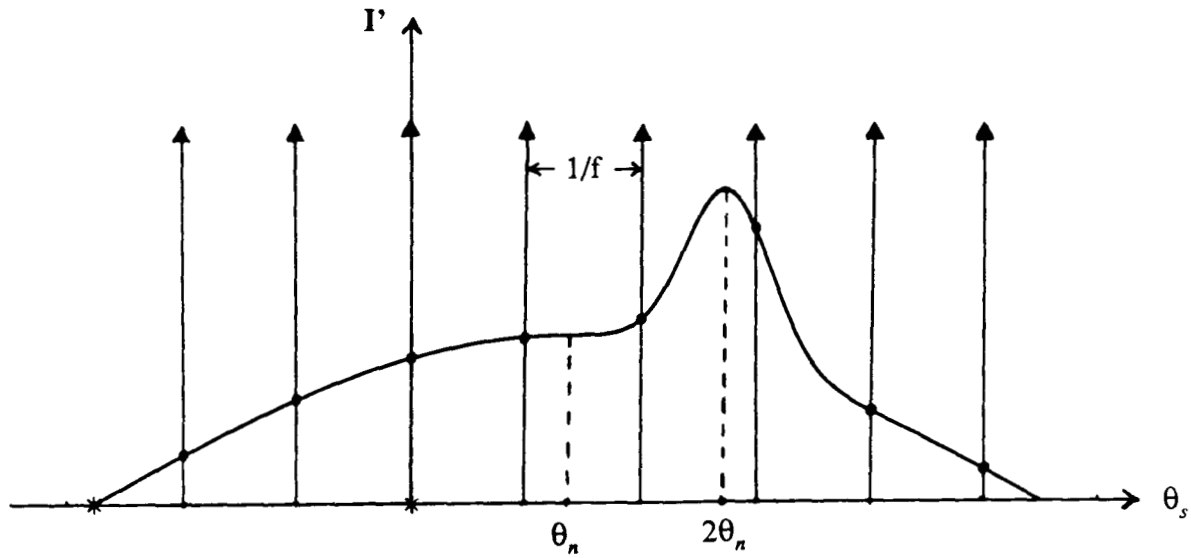

Figure 4: Sampling the modified photometric function.

3 Extracting Shape and Reflectance of Surfaces

Given the set of image intensities $\{I'_i\}$, we want to determine the surface orientation θ_n and the strengths A' and B' of the Lambertian and specular components of reflection. The shape and reflectance properties extracted at each surface point are solely based on the image

[2]It is assumed that the period of the photometric function that contains specular intensities is small compared to the total width of the photometric function. Therefore, sampling frequencies that ensure the detection of specular intensities will provide a sufficient number of Lambertian intensity samples.

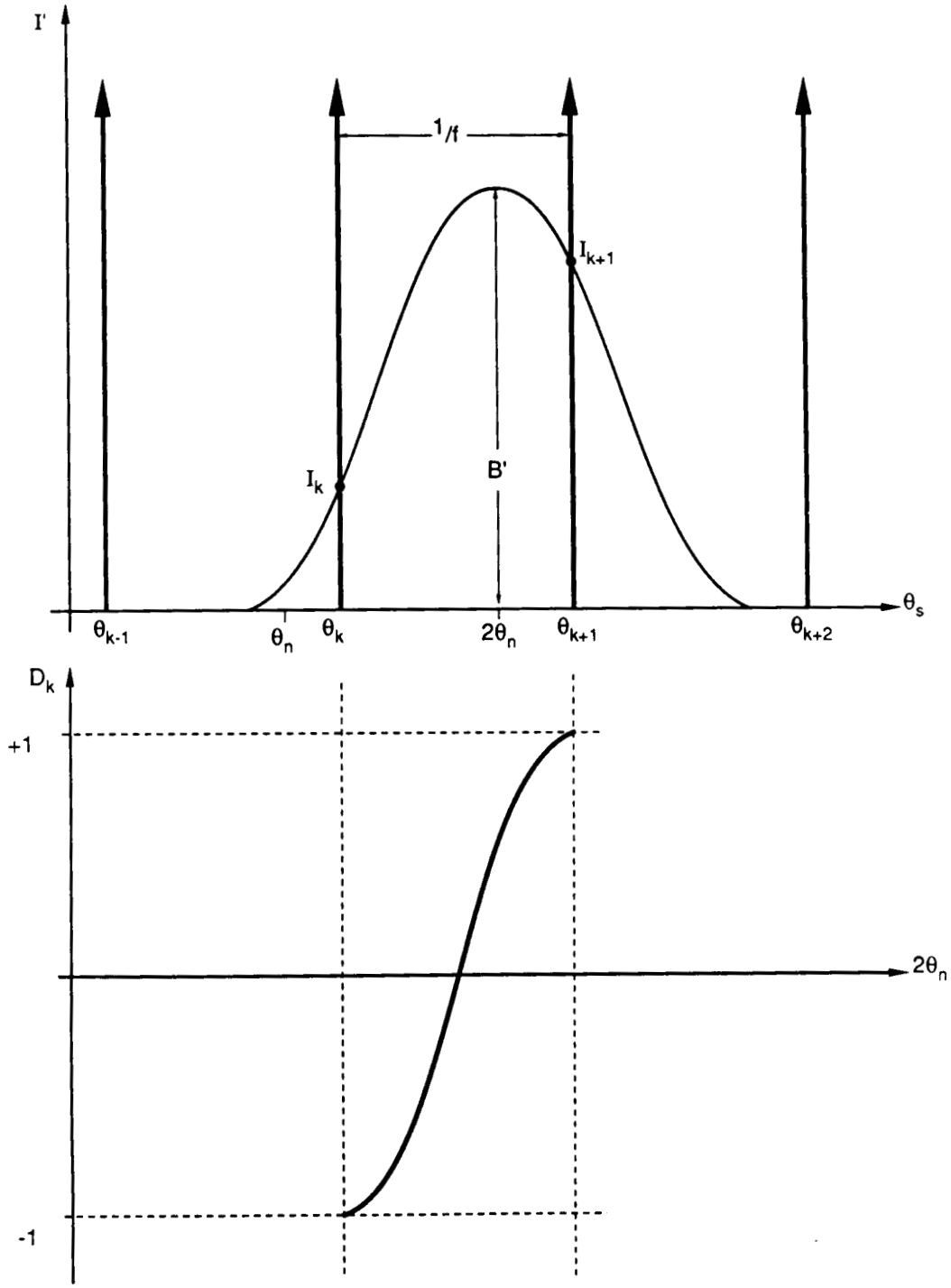

Figure 5: For specular surfaces, the normalized brightness difference function $D_k(2\theta_n)$ establishes a unique mapping from image intensities I'_k and I'_{k+1} to surface orientation θ_n.

Samples I'_i of the photometric function $I'(\theta_s)$ are related to the extended source position θ_i as:

$$I'_i = B' L(2\theta_n, \theta_i) . \tag{22}$$

Since B' is unknown, it is not possible to find the peak position of $I'(\theta_s)$ from a single sample. However, since we know the shape of $I'(\theta_s)$, we can find the peak of $I'(\theta_s)$ from two samples of $I'(\theta_s)$, as shown in Figure 5. Consider the samples I'_k and I'_{k+1} that result from extended sources positioned at θ_k and θ_{k+1}, respectively. Let us assume that $\theta_{k+1} = \theta_k + \alpha$. We see that when θ_n increases, $I'(\theta_s)$ shifts to the right, I'_k decreases, and I'_{k+1} increases. Similarly, when θ_n decreases, $I'(\theta_s)$ shifts to the left, I'_k increases, and I'_{k+1} decreases.

In order to determine the surface orientation θ_n and the specular strength B' from the two non-zero image intensities I'_k and I'_{k+1}, we define the normalized brightness difference function $D_k(2\theta_n)$ as [13]:

$$D_k(2\theta_n) = \frac{L(2\theta_n, \theta_{k+1}) - L(2\theta_n, \theta_k)}{L(2\theta_n, \theta_{k+1}) + L(2\theta_n, \theta_k)} . \tag{23}$$

The analytic expressions for $L(2\theta_n, \theta_k)$ and $L(2\theta_n, \theta_{k+1})$ (Appendix A) may be substituted in equation 23. As shown in Figure 5, as $2\theta_n$ increases from θ_k to θ_{k+1}, $D_k(2\theta_n)$ varies monotonically from $D_k(\theta_k) = -1$ to $D_k(\theta_{k+1}) = 1$. Therefore, if the value of $D_k(2\theta_n)$ can be computed from measured image intensities, we can uniquely determine the orientation θ_n.

Given the image intensity set $\{I'_i\}$ at a specular surface point, the non-zero image intensities in the set are first determined. If only a single intensity value, for instance I'_k, is greater than zero, then we know that $2\theta_n = \theta_k$. If two image intensities, for instance I'_k and I'_{k+1}, are greater than zero, the normalized brightness difference function $D_k(2\theta_n)$ is determined from I'_k and I'_{k+1} by using equations 22 and 23:

$$D_k(2\theta_n) = \frac{I'_{k+1} - I'_k}{I'_{k+1} + I'_k} . \tag{24}$$

Given the value of $D_k(2\theta_n)$, we can find orientation θ_n by using equation 23.

As shown above, surface orientation θ_n is computed without prior knowledge of the strength B' of the specular component of reflection. Once θ_n is found, B' is determined by using equation 22:

$$B' = \frac{I'_k}{L(2\theta_n, \theta_k)} . \tag{25}$$

3.3 Hybrid Surfaces

In practice, purely Lambertian or purely specular surfaces are unlikely occurrences. A large number of surfaces may be classified as hybrid surfaces whose reflectance models

are composed of both Lambertian and specular components. Surfaces of plastic objects are examples of hybrid surfaces. For extended source illumination, the photometric function for these surfaces is given by equation 16. The strengths A' and B' of the Lambertian and specular components may vary from surface point to surface point. At each surface point, we want to determine A', B', and orientation θ_n from the measured samples $\{I'_i$: i=1,2,.....M$\}$ of the photometric function. To this end, we will develop an algorithm that attempts to separate the Lambertian and specular components of each measured image intensity, and computes surface orientations by using the methods given above for Lambertian and specular surfaces.

The extraction algorithm is based on two constraints, namely, the *sampling frequency constraint* and the *unique orientation constraint.* By sampling the modified photometric function at the *minimum sampling frequency* f_{min}, we can ensure that only two consecutive image intensities in the intensity set $\{I'_i\}$ contain non-zero specular components of intensity. For each k in the interval $0 < k < M$, I'_k and I'_{k+1} are hypothesized as being the two intensities that are corrupted by specular components. All remaining intensities in the set $\{I'_i$: i=1,2,.....M$\}$ must represent only Lambertian components of reflection. These intensities are used to compute the surface orientation θ_{nl} and the Lambertian strength A'. The Lambertian components IL'_k and IL'_{k+1} are determined and used to separate the specular components IS'_k and IS'_{k+1} from I'_k and I'_{k+1}, respectively. The surface orientation θ_{ns} and specular strength B' are computed from IS'_k and IS'_{k+1} by using the specular reflectance model.

Next, the physical constraint that each surface point has a *unique orientation* is exploited. An estimate θ_{nk} of the orientation is found as a weighted average of the orientations θ_{nl} and θ_{ns}. The weights are proportionate to the strengths of the two components of reflection. We support this method of weight selection because the surface orientation that is computed from intensities resulting from the stronger of the two reflection components is less sensitive to image noises and is, therefore, more reliable. An orientation error e_k is found by comparing θ_{nk} with θ_{nl} and θ_{ns}. The orientation error is computed for every k, where $0 < k < M$. The surface orientation and reflectance strengths computed for the value of k that minimizes e_k are assigned to the surface point under consideration. This process is repeated for all points on the object surface.

It is important to note that the following algorithm is not only capable of determining shape and reflectance properties of hybrid surface but also Lambertian and specular surfaces.

Extraction Algorithm

Step 1: Let k = 1 and e_0 equal a large positive number.

Step 2: Hypothesize that image intensities I'_k and I'_{k+1} consist of specular components of

reflection. All intensities I'_i, where $i \neq k$ and $i \neq k+1$, and the Lambertian component of the photometric function are used to compute the surface orientation θ_{nl} and Lambertian strength A'_k (section 3.1).

Step 3: The specular components IS'_k and IS'_{k+1} are separated from the image intensities I'_k and I'_{k+1}:

$$\begin{aligned} IS'_k &= I'_k - A'_k \cos(\theta_k - \theta_{nl}), \\ IS'_{k+1} &= I'_{k+1} - A'_k \cos(\theta_{k+1} - \theta_{nl}). \end{aligned} \tag{26}$$

If $IS'_k < 0$ or $IS'_{k+1} < 0$, set $k = k + 1$ and go to step 2.

Step 4: The surface orientation θ_{ns} and the strength of the specular reflection B'_k are determined by using specular intensities IS'_k and IS'_{k+1} and the specular component of the photometric function (section 3.2).

Step 5: We have separated the Lambertian and specular components from the set of measured image intensities and computed the surface orientations θ_{nl} and θ_{ns} by using the Lambertian and specular reflectance models, respectively. The best estimate of surface orientation, for the k^{th} iteration, is determined as:

$$\theta_{nk} = \frac{A'_k \theta_{nl} + B'_k \theta_{ns}}{A'_k + B'_k}. \tag{27}$$

The orientation at the surface point under consideration is unique. Therefore, if we have correctly selected intensities I'_k and I'_{k+1} as the two intensities that contain non-zero specular components, then θ_{nl}, θ_{ns}, and θ_{nk} must be equal to one another. An orientation error e_k is defined as:

$$e_k = \frac{A'_k |\theta_{nl} - \theta_{nk}| + B'_k |\theta_{ns} - \theta_{nk}|}{A'_k + B'_k}. \tag{28}$$

Step 6: If $e_k < e_{k-1}$, then:

$$\begin{aligned} \theta_n &= \theta_{nk}, \\ A' &= A'_k, \\ B' &= B'_k. \end{aligned} \tag{29}$$

If $k < M-1$, set $k = k + 1$ and go to step 2. Else, stop.

4 Extension to Three Dimensions

In the previous sections, photometric sampling was described in two dimensions. Figure 6 illustrates the point source illumination of a surface element in three dimensions. All vectors are represented by the two parameters θ and ψ where θ is the azimuth angle and ψ is the longitudinal angle. We shall refrain from presenting detailed derivations of all the equations for the three-dimensional case and rather describe the final forms of the relevant equations.

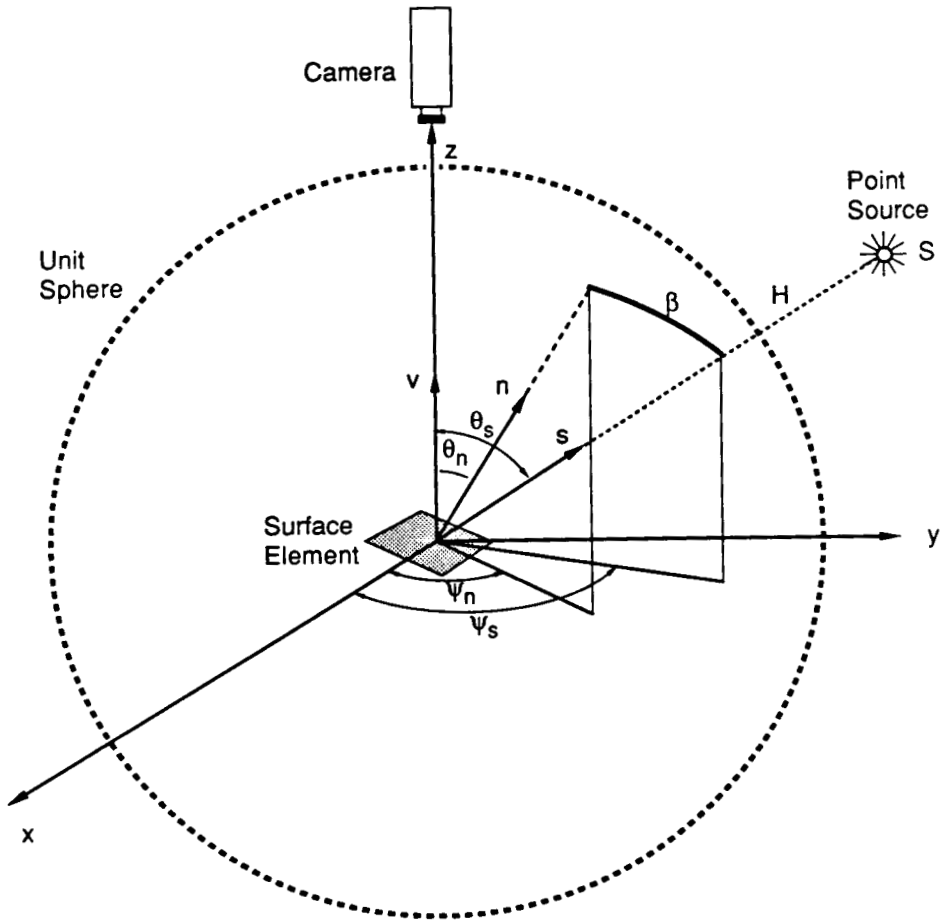

Figure 6: Surface illumination and imaging in three dimensions. Surface orientation and source direction are represented by the two parameters θ and ψ.

4.1 Basic Photometric Function

In Figure 6, the point source S is located in the direction $(\theta_s, \psi_s)$and the surface normal vector **n** points in the direction (θ_n, ψ_n). The Lambertian component of the basic photometric function is a cosine function of the angle β between the surface normal vector **n** and the point source direction vector **s**. We have assumed the specular reflectance model to be a unit impulse function. Since directions are represented by the two parameters θ and ψ, the specular component of the photometric function for the three-dimensional geometry is expressed as a double-impulse function. Therefore, for point source illumination, the three-dimensional photometric function may be written as:

$$I = A\,cos\beta + B\,u(\theta_s - 2\theta_n)\,u(\psi_s - \psi_n)\,. \tag{30}$$

By using spherical trigonometry, the term $cos\beta$ may be determined from the surface normal direction and the source direction as:

$$cos\beta = cos\theta_n\,cos\theta_s + sin\theta_n\,sin\theta_s\,cos(\psi_s - \psi_n)\,. \tag{31}$$

4.2 Photometric Function for Extended Sources

The radiance function for a three-dimensional extended source is given in Appendix A.2. The photometric function for extended source illumination is obtained by convolving the basic photometric function $I'(\theta,\psi)$ with the extended source radiance function $L(\theta, \psi, \theta_s, \psi_s)$. Since each radiance function $L(\theta, \psi, \theta_s, \psi_s)$ is symmetric about the corresponding source direction (θ_s, ψ_s), the Lambertian component of the modified photometric function is a cosine function of the angle between the extended source direction (θ_s, ψ_s) and the surface normal direction (θ_n, ψ_n). The specular component of the modified photometric function is proportional to the extended source radiance in the direction $(2\theta_n,\psi_n)$. Therefore, the photometric function for surface illumination by the extended source $L(\theta, \psi, \theta_s, \psi_s)$ is:

$$I' = A'\,cos\beta + B'\,L(2\theta_n, \psi_n, \theta_s, \psi_s)\,. \tag{32}$$

4.3 Sampling

Samples of the modified photometric function can be obtained by illuminating the object surface from different source directions. An extended source can be moved to different locations around the object and an image of the object obtained for each source direction. Alternatively, a number of extended sources can be distributed around the object and an image of the object taken for each extended source. A uniform sampling of the photometric

function may be obtained by distributing extended sources in a tessellation that results from projecting onto the unit sphere regular polyhedra whose centers coincide with that of the sphere [1].

4.4 Extracting Shape and Reflectance of Surfaces

Though the basic principle used by the extraction algorithm remains unchanged for the three-dimensional case, a few modifications are necessary to accommodate for the additional degree of freedom given to surface orientation by the parameter ψ. If the object surface is known to be purely Lambertian, an error minimization similar to the one used in the two-dimensional case may be used to fit the Lambertian reflectance model to the image intensities $\{I'_i\}$ to determine the Lambertian strength A' and the surface orientation (θ_n, ψ_n). On the other hand, if the surface is purely specular, orientation can be determined from the non-zero photometric samples. If extended sources are distributed in the icosahedron tessellation, any three adjacent point sources will constitute the vertices of an equilateral triangle. If adjacent sources are separated by the source termination angle α, the samples measured at a specular surface point will have three non-zero intensities (see Appendix A.2).

The extraction algorithm for the three-dimensional geometry is once again based on the sampling frequency and unique orientation constraints. It assumes that only three image intensities I'_k, I'_{k+1}, and I'_{k+2}, generated by three adjacent extended light sources, can contain non-zero specular components of intensity. All remaining intensities in the set $\{I'_i\}$ must represent only Lambertian reflection. These intensities are used to compute the surface orientation (θ_{nl}, ψ_{nl}) and the Lambertian strength A'_k. The Lambertian components IL'_k, IL'_{k+1}, and IL'_{k+2} are computed and used to separate the specular components IS'_k, IS'_{k+1}, and IS'_{k+2} from I'_k, I'_{k+1}, and I'_{k+2}, respectively. Next, the surface orientation (θ_{ns}, ψ_{ns}) and the specular strength B'_k are computed from IS'_k, IS'_{k+1}, and IS'_{k+2} by using the the specular reflectance model. We use the physical constraint that each surface point has a unique surface orientation. An estimate (θ_{nk}, ψ_{nk}) of the orientation is found as a weighted sum of the orientations (θ_{nl}, ψ_{nl}) and (θ_{ns}, ψ_{ns}), and an orientation error is computed as a function of the deviations of (θ_{nk}, ψ_{nk}) from (θ_{nl}, ψ_{nl}) and (θ_{ns}, ψ_{ns}). This process is repeated for every set of three adjacent sources, and the surface orientation and reflectance strengths that minimize the orientation error are assigned to the surface point. The extraction algorithm is executed for each point on the object surface.

is shown in Figure 8. A 14-inch diameter lamp shade is used as the spherical diffuser, and extended light sources are generated on the diffuser's surface by illuminating it using incandescent light bulbs. The object is placed at the center of the diffuser and is viewed by a camera through a 1-inch diameter hole in the surface of the diffuser. The current set-up uses a WV-22 model Panasonic CCD camera that has a 512×480 pixel resolution. The complete imaging system, comprising of lenses and camera, has a physical resolution of 0.002 inches per pixel width. In the current implementation, the light bulbs, camera, and object are all placed in the same plane. This two-dimensional set-up is only capable of measuring the orientation of surface normal vectors that lie on a single plane in orientation space. For each extended source, an image of the object is digitized and stored in memory. The sequence of object images, generated by scanning the array of extended sources, is processed using the extraction algorithm that is coded on a 3/60 SUN work-station. The surface orientation and reflectance information produced by the extraction algorithm is color-coded and displayed on a color monitor.

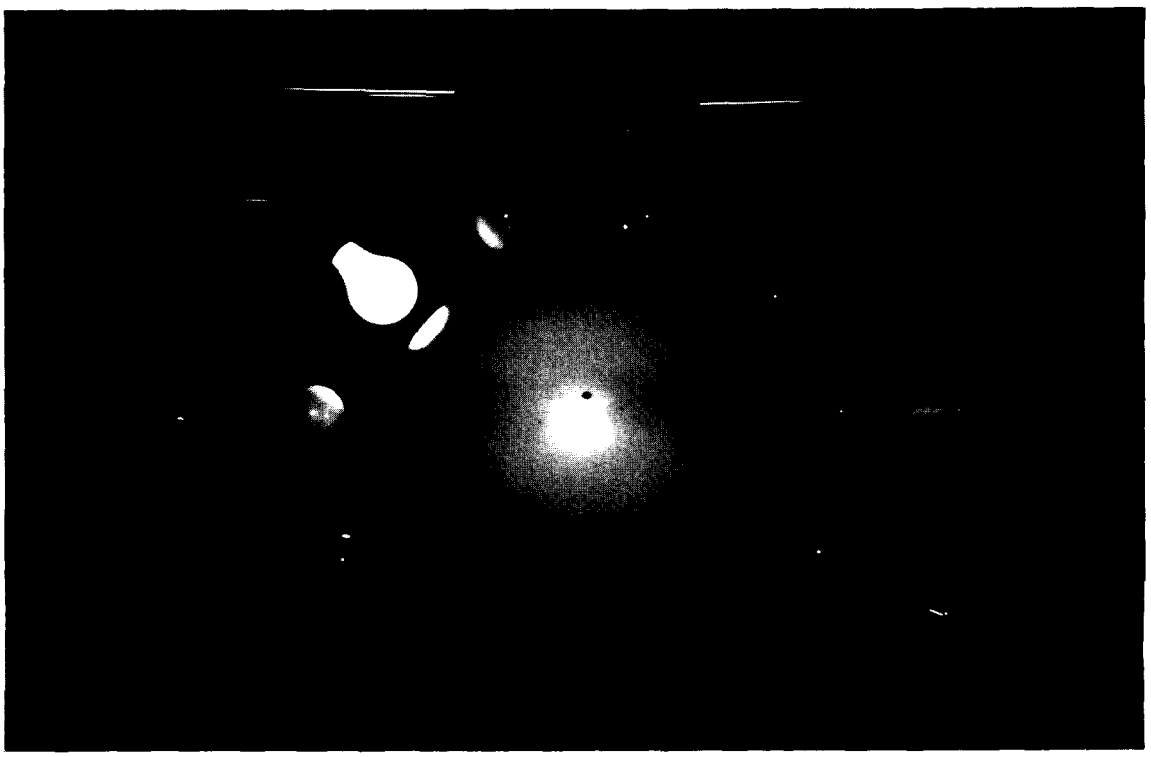

Figure 8: Photograph of the experimental set-up used to demonstrate the photometric sampling concept.

5.2 Sampling Photometric Functions

The experimental set-up was used to extract the surface properties of a number of objects. In order to show that the measured intensities are consistent with the theory developed in the previous section, we will first present plots of measured samples of the photometric function for surfaces of different reflectance properties. Figure 9 shows the image intensities that were measured at a single pixel, plotted as a function of the extended source direction. The measured intensity values are represented by black dots. The surface point under consideration is specular and, as expected, only two consecutive sources in the entire array produce image intensities that are significantly greater than zero. Figure 10 shows a similar plot for a Lambertian surface point. To prove that the intensities describe a cosine function, the cosine function that best fits the intensities is superimposed on the same plot and is represented by a solid curve. The measured intensities are observed to lie in close proximity to the cosine function. Since Lambertian and specular surfaces produced intensity values that appeared to be consistent with their reflectance models, similar experiments were conducted on hybrid surfaces. Figure 11 shows photometric samples measured at a point on the surface of a plastic object whose reflectance model includes both Lambertian and specular components. The orientation of the surface point was known a-priori, and thus the two measured samples that were expected to consist of both Lambertian and specular intensities were identified and are marked in the figure as "L+S". All remaining image intensities result from Lambertian reflection and are marked in the figure as "L". The cosine function that best fits the Lambertian intensities is represented by the solid curve. The specular components were extracted from the two intensities that are marked as "L+S". Two estimates of surface orientation were computed using the Lambertian and the specular components of the image intensities. Both computed orientations were found to be within 3 degrees of the actual orientation value.

5.3 Lambertian, Specular, and Hybrid Surfaces

On the basis of the above experiments, the extraction algorithm was implemented and surface properties of a large number of objects were extracted. Figures 12 through 31 show the results of the extraction method applied to objects of varying surface reflectance properties. For each object, a photograph of the object is followed by a needle map and two reflectance images produced by the extraction algorithm. A needle map is a representation of surface orientations. At each point on a needle map, the length of the needle is proportional to the tilt of the surface away from the viewing direction of the camera. The direction in which each needle points is determined by locating the starting point of the needle. All needles originate from the dots that constitute the resolution grid of the needle map. In all the needle maps shown in this paper, the needles always appear horizontally oriented because

only a two-dimensional illumination geometry has been implemented. Therefore, only those surface normal vectors that are oriented parallel to the plane of illumination can be measured. The reflectance properties of the surfaces are given by two images, namely, the Lambertian strength image and the specular strength image. The intensity at each pixel, in either of these two images, is proportional to the strength of the reflectance component the image represents. For example, a Lambertian surface point would have maximum intensity in the Lambertian strength image and zero intensity in the specular strength image, and specular surface point would have maximum intensity in the specular strength image and zero intensity in the Lambertian strength image. Hybrid points would have non-zero intensities in both Lambertian and specular strength images.

The object shown in Figure 12 is a prism and its surface is Lambertian. The object shown in Figure 16 is cylindrical and its surface is also Lambertian. Figure 20 shows a prism that has a highly specular surface. An interesting application for the proposed method is seen in objects such as the one shown in Figure 24. The object is a metal bolt that has a hexagonal head, and the painted surface of the head is Lambertian in reflection. The threaded section of the bolt has a specular surface. Surface orientations are measured only along the thin edges of the threads since surface orientations in the grooves between threads lie outside the range of orientations that the current two-dimensional system is capable of measuring. While generating needle maps, surface orientations are sampled to make room for the display of needles. During sampling, a considerable number of orientations measured on the threads of the bolt are lost. In order to get a better picture of the shape of the threaded section, orientations measured on a few threads are displayed at a higher resolution.

All the above experiments were conducted on surfaces constituting points that were either Lambertian or specular. A major advantage of the photometric sampling method, over all existing shape extraction techniques, lies in its ability to determine the shape and reflectance of hybrid surfaces. Plastic objects seem to fit the description of hybrid surfaces given earlier in this paper. Figure 28 shows the photo of a cylindrical plastic object. The needle map of the object, generated by the extraction algorithm, is consistent with the actual shape. As expected, non-zero Lambertian and specular strengths are noted in the reflection images of the plastic surface. An important feature of all the above results is that the surface properties computed at a pixel are solely based on the intensities recorded at that pixel. The needle maps and reflectance images have not been subjected to any filtering operations.

5.4 Measurement Accuracy and Processing Time

A simple error analysis was conducted to estimate the measurement accuracy of the current set-up. In the results obtained so far, the surface orientations were found to be within 4

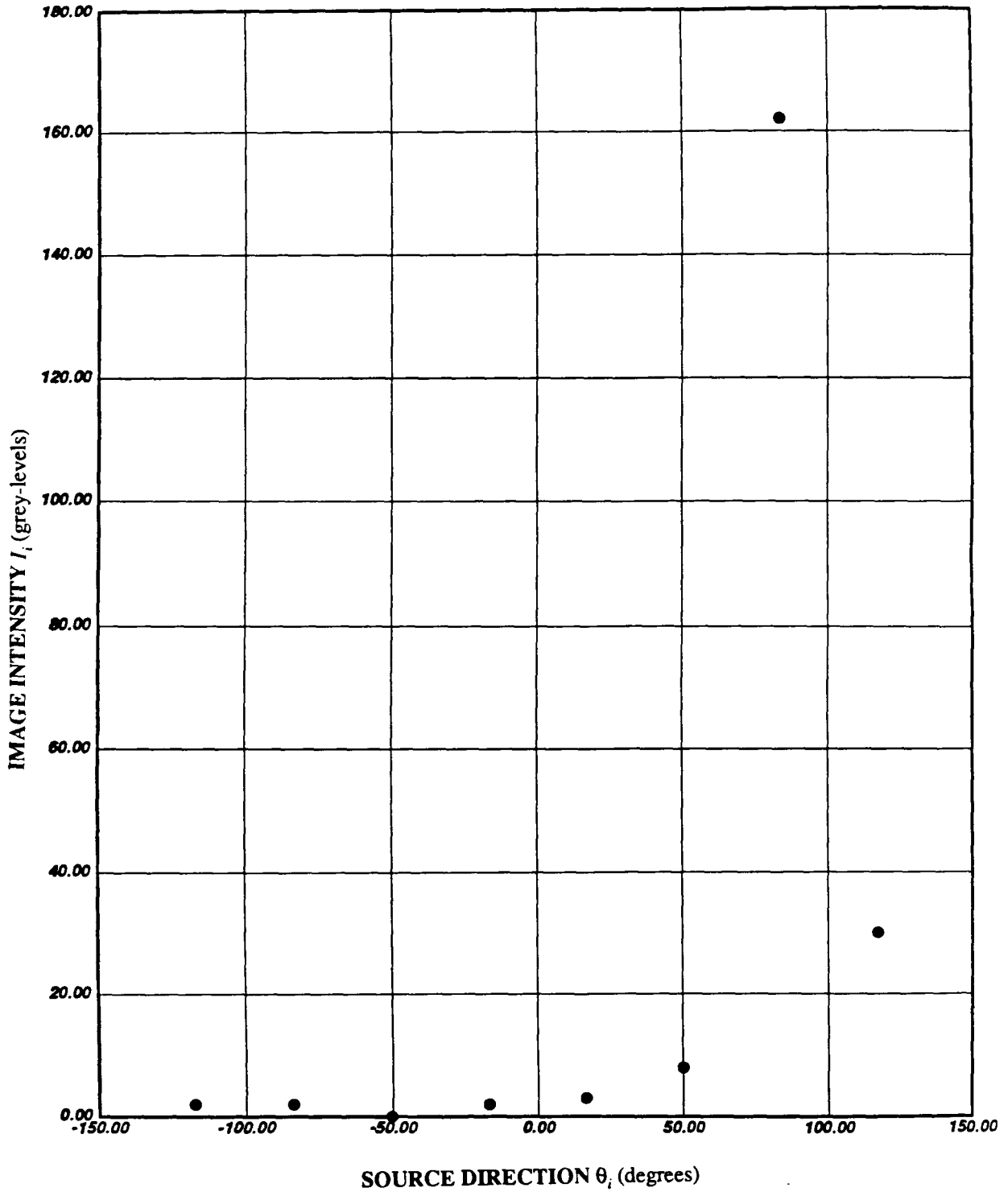

Figure 9: Photometric samples measured at a specular surface point. The measured intensities I'_i are plotted as a function of the extended source direction θ_i.

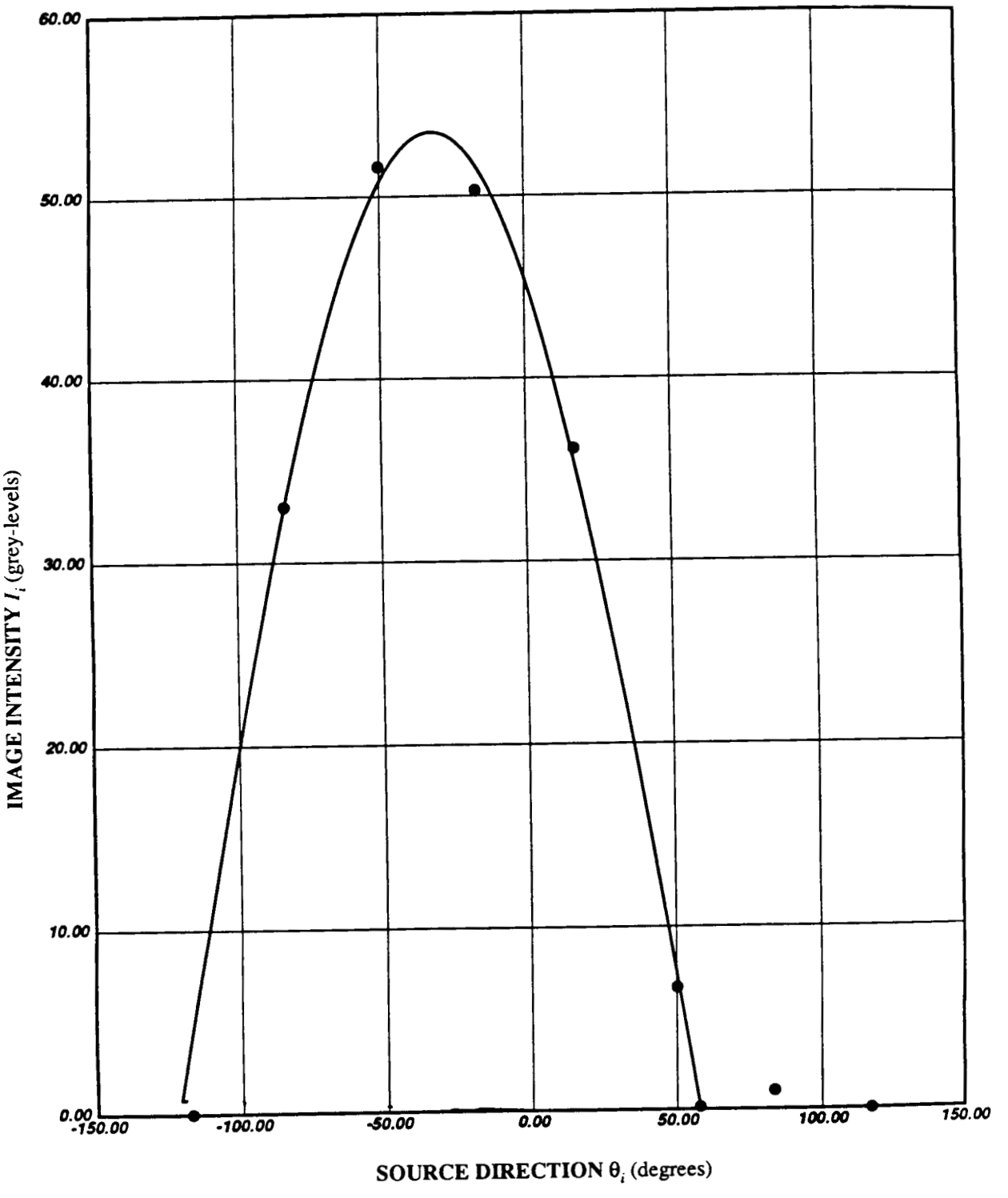

Figure 10: Photometric samples measured at a Lambertian surface point. The cosine function that best fits the measured intensities is shown as a solid curve.

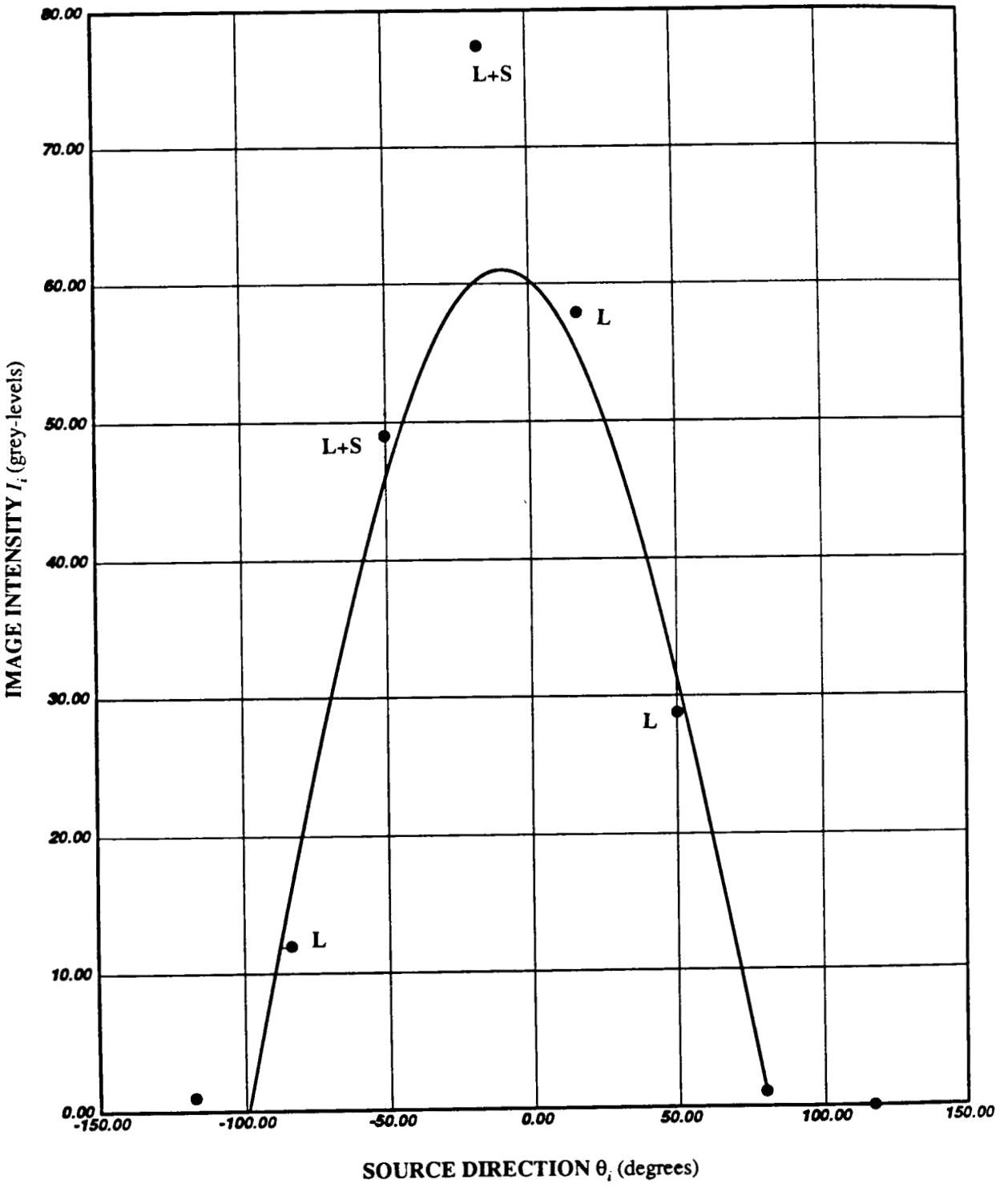

Figure 11: Photometric samples measured at a hybrid surface point. By using the known orientation of the surface point, the two intensities corrupted by specular reflections were identified and marked "L+S". The remaining points result solely from Lambertian reflection and the cosine function that best fits these points is shown as a solid curve.

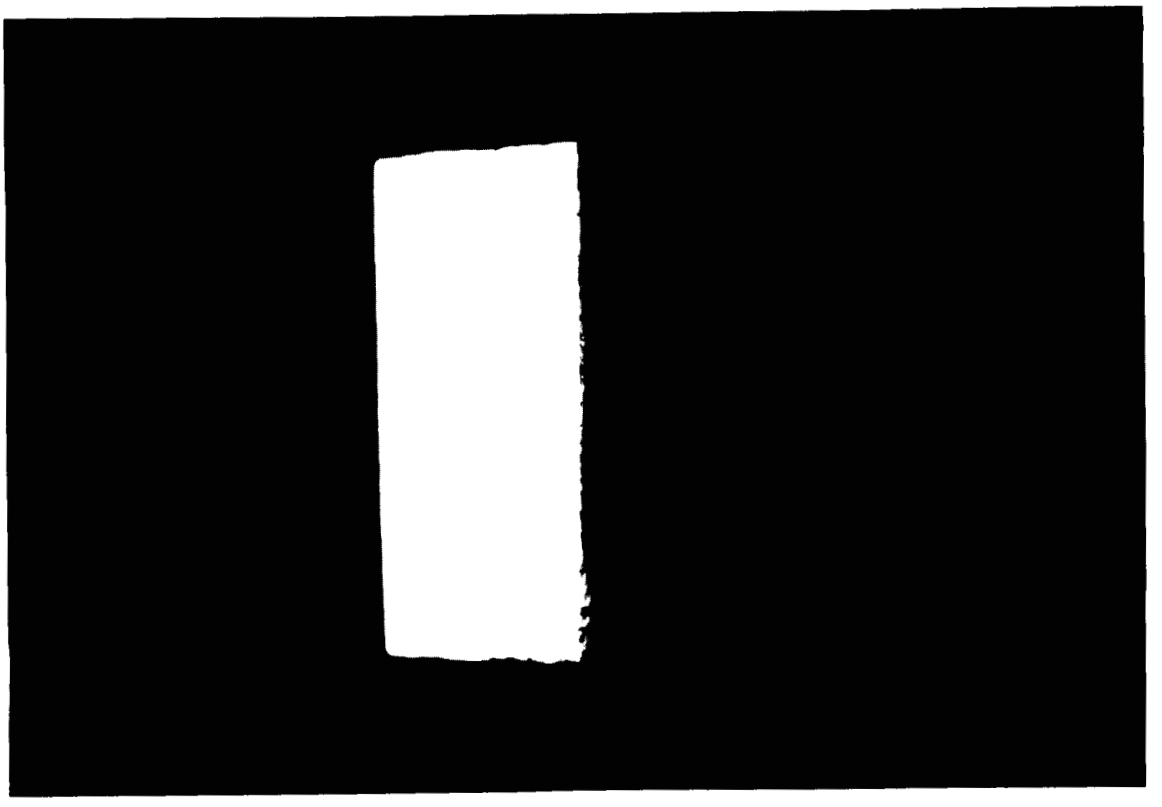

Figure 12: Photo of a prism that has a Lambertian surface.

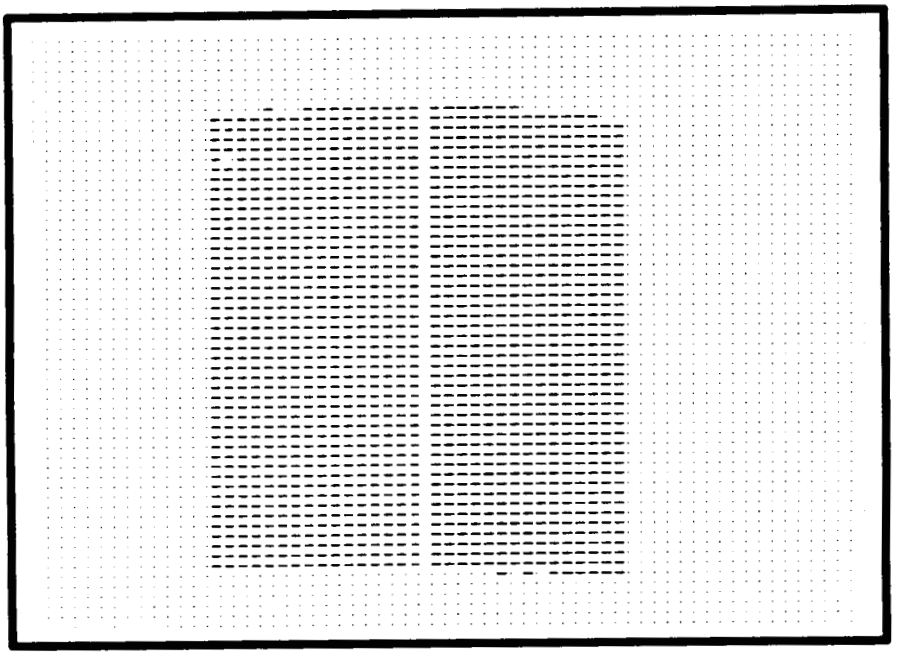

Figure 13: Needle map for the object shown in Figure 12.

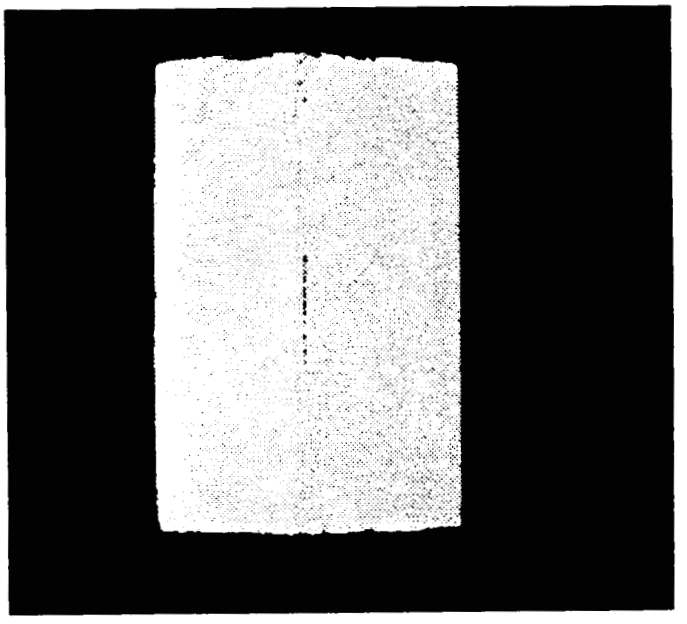

Figure 14: Lambertian strength image for the object shown in Figure 12.

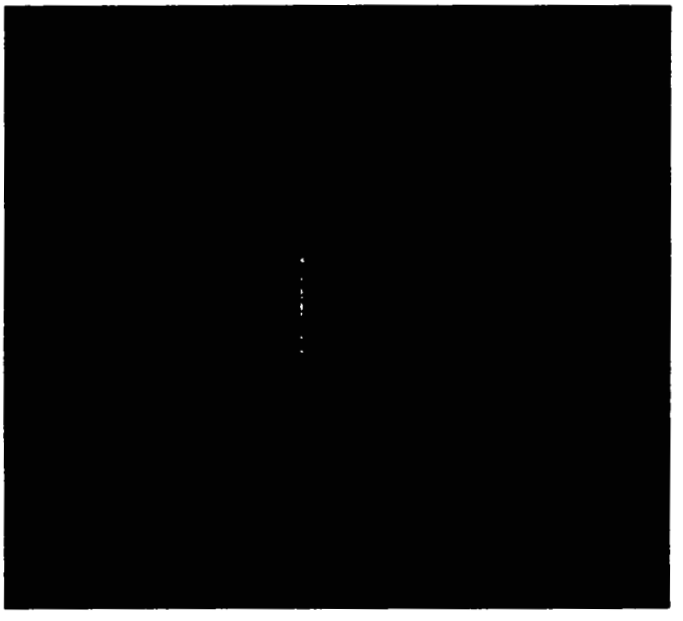

Figure 15: Specular strength image for the object shown in Figure 12.

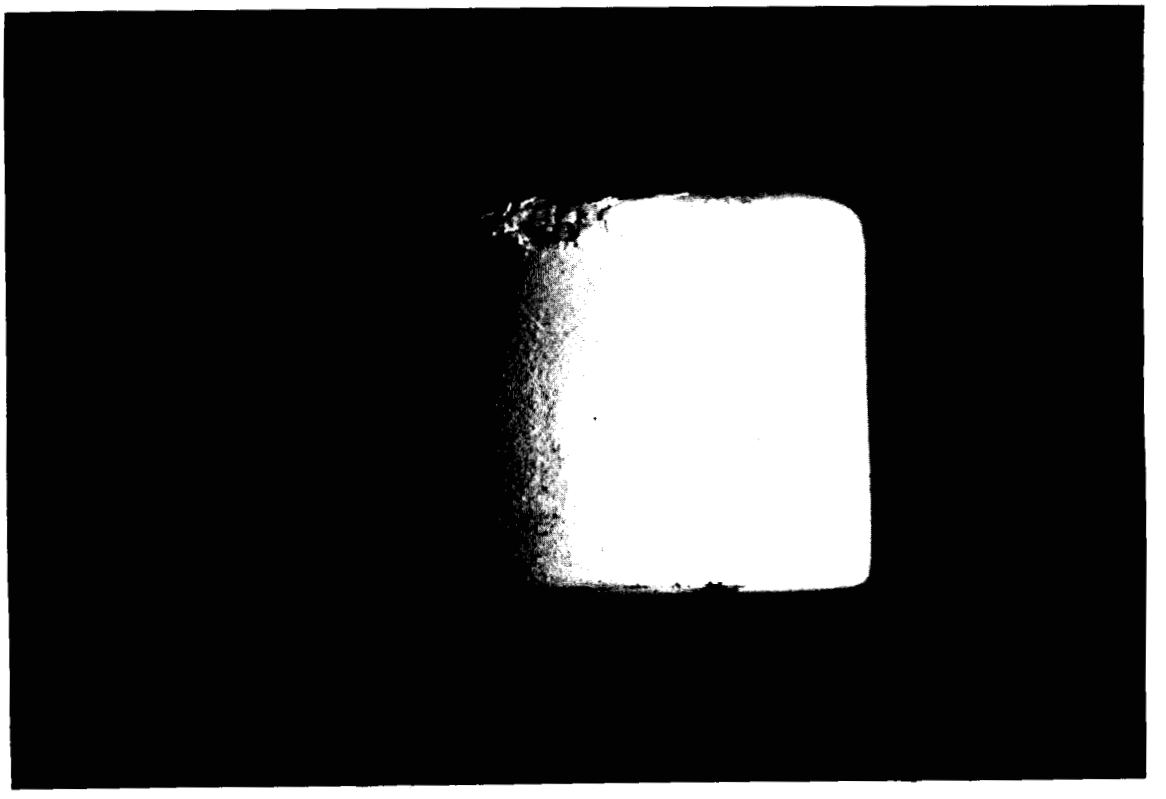

Figure 16: Photo of a cylindrical object that has a Lambertian surface.

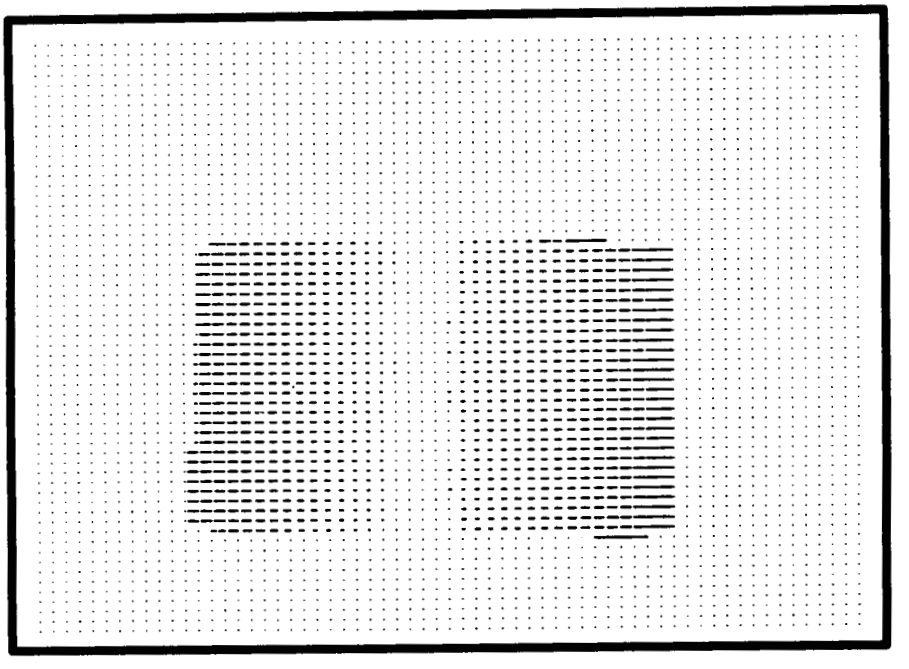

Figure 17: Needle map for the top cylindrical surface of the object shown in Figure 16.

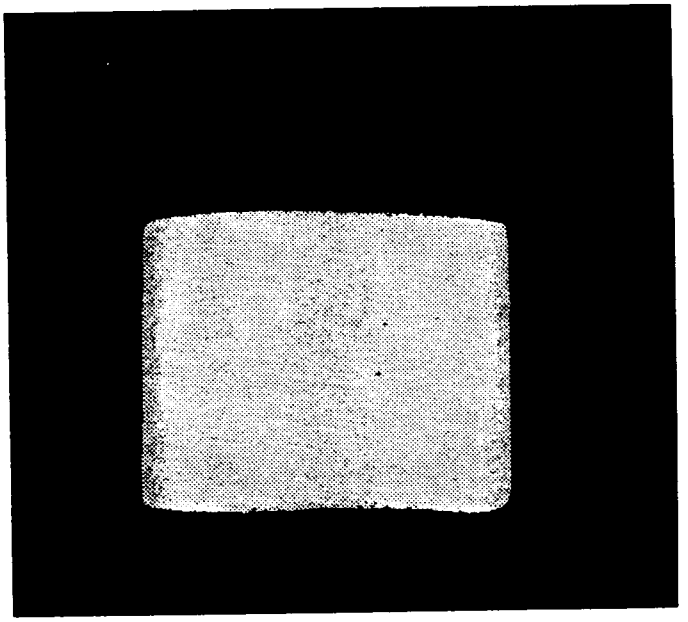

Figure 18: Lambertian strength image for the object shown in Figure 16.

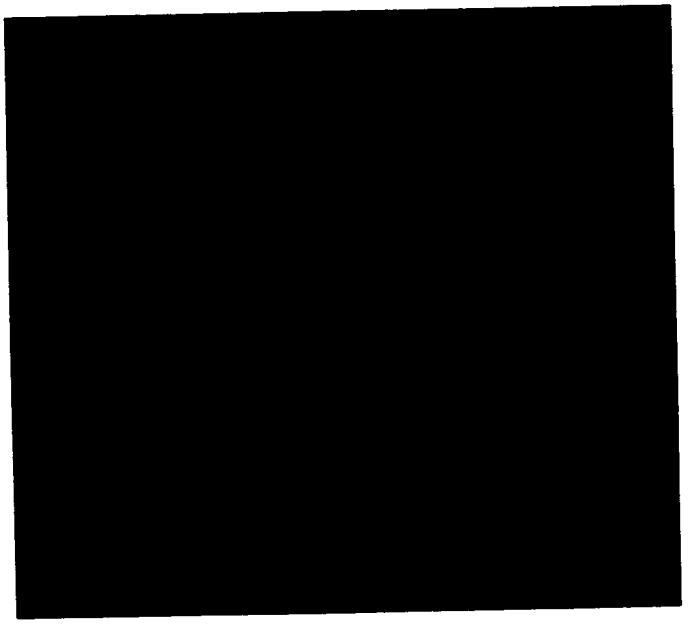

Figure 19: Specular strength image for the object shown in Figure 16.

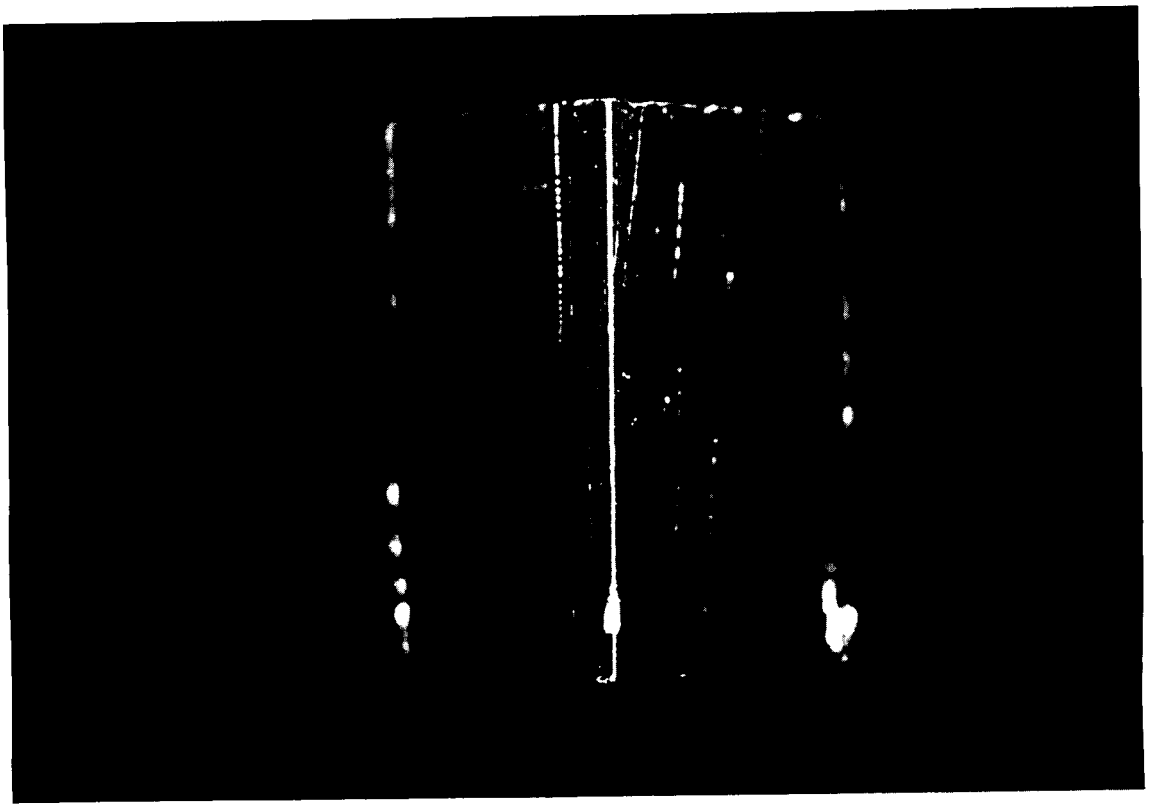

Figure 20: Photo of a prism that has a specular surface.

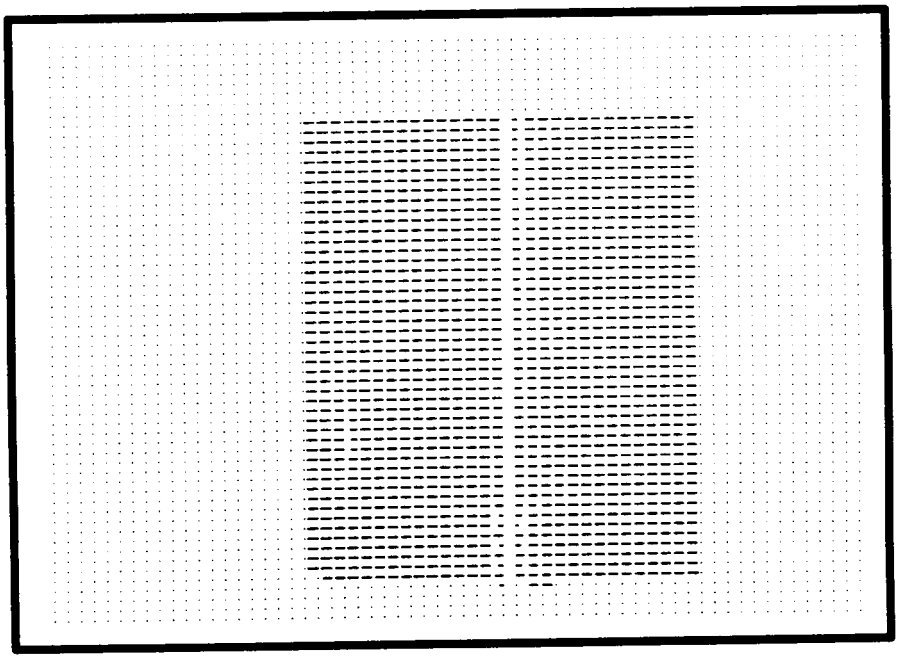

Figure 21: Needle map for the object shown in Figure 20.

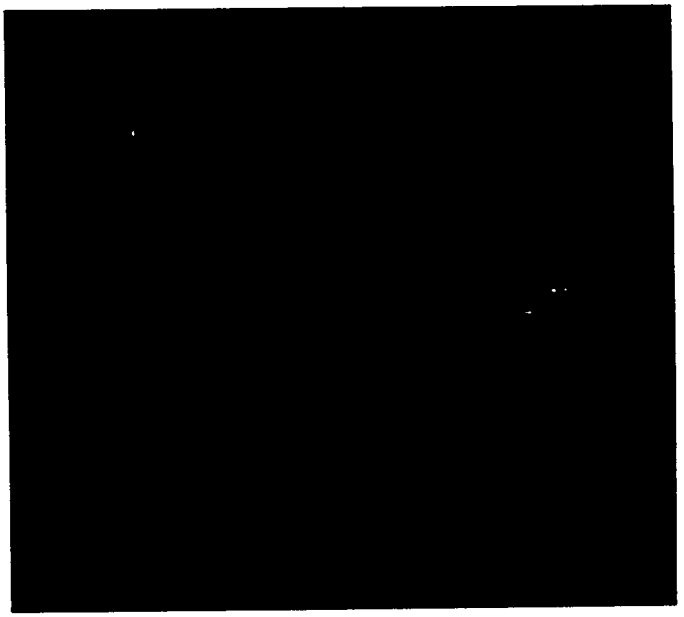

Figure 22: Lambertian strength image for the object shown in Figure 20.

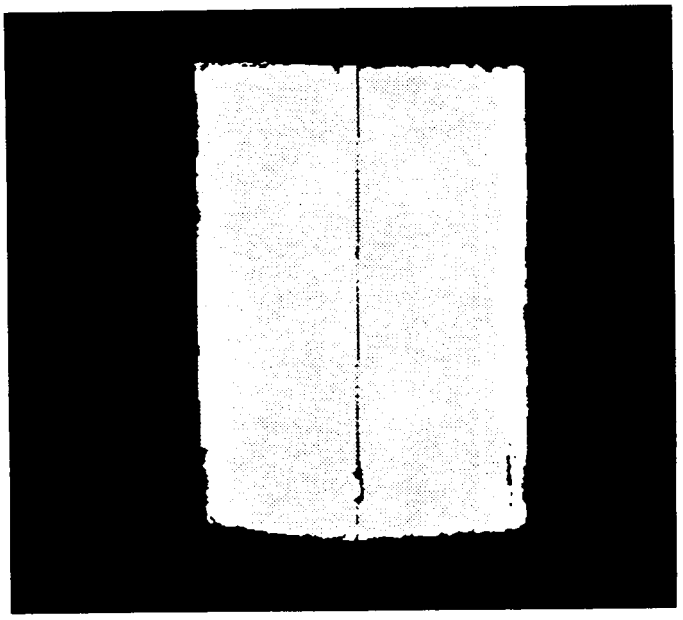

Figure 23: Specular strength image for the object shown in Figure 20.

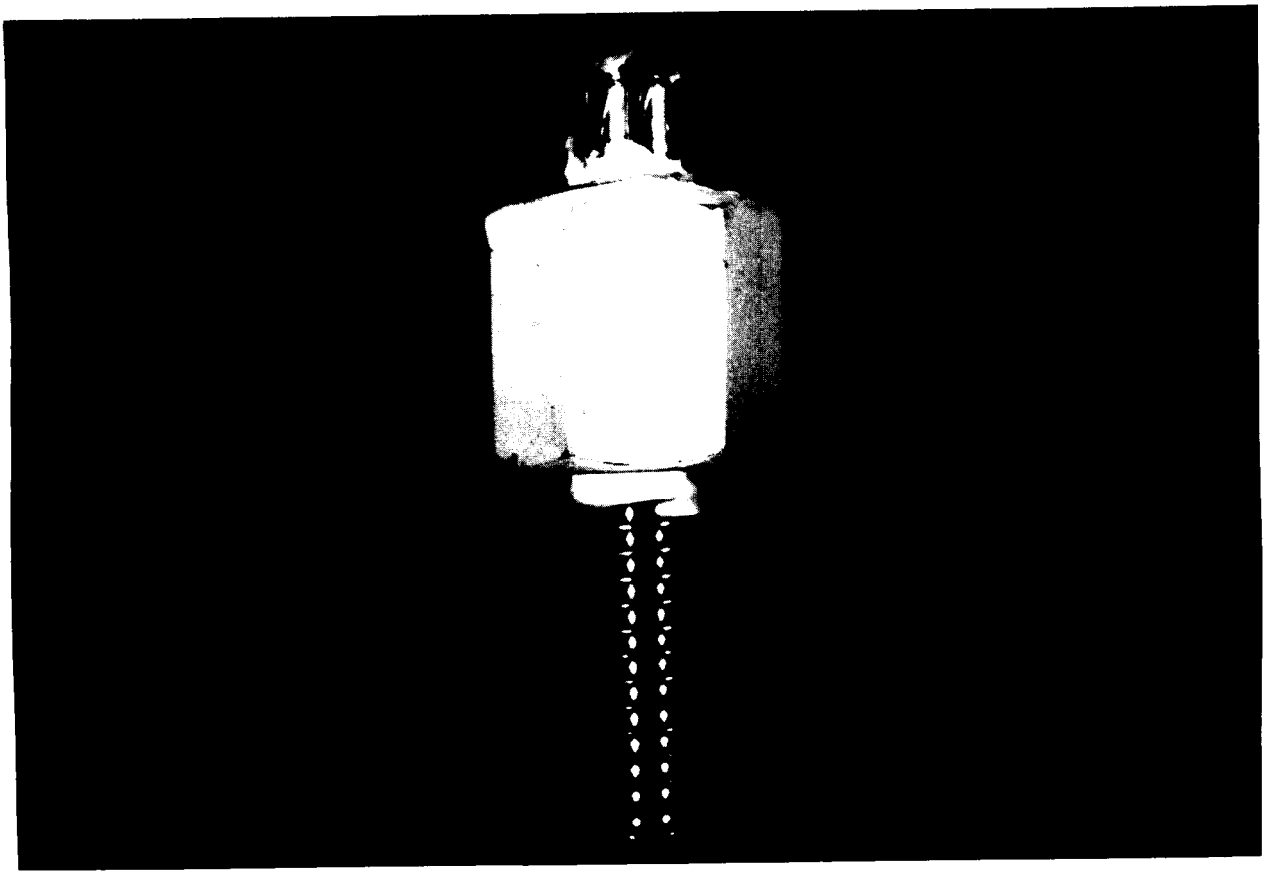

Figure 24: Photo of a metal bolt. The head of the bolt is hexagonal and has a Lambertian surface, while the threaded section of the bolt has a specular surface.

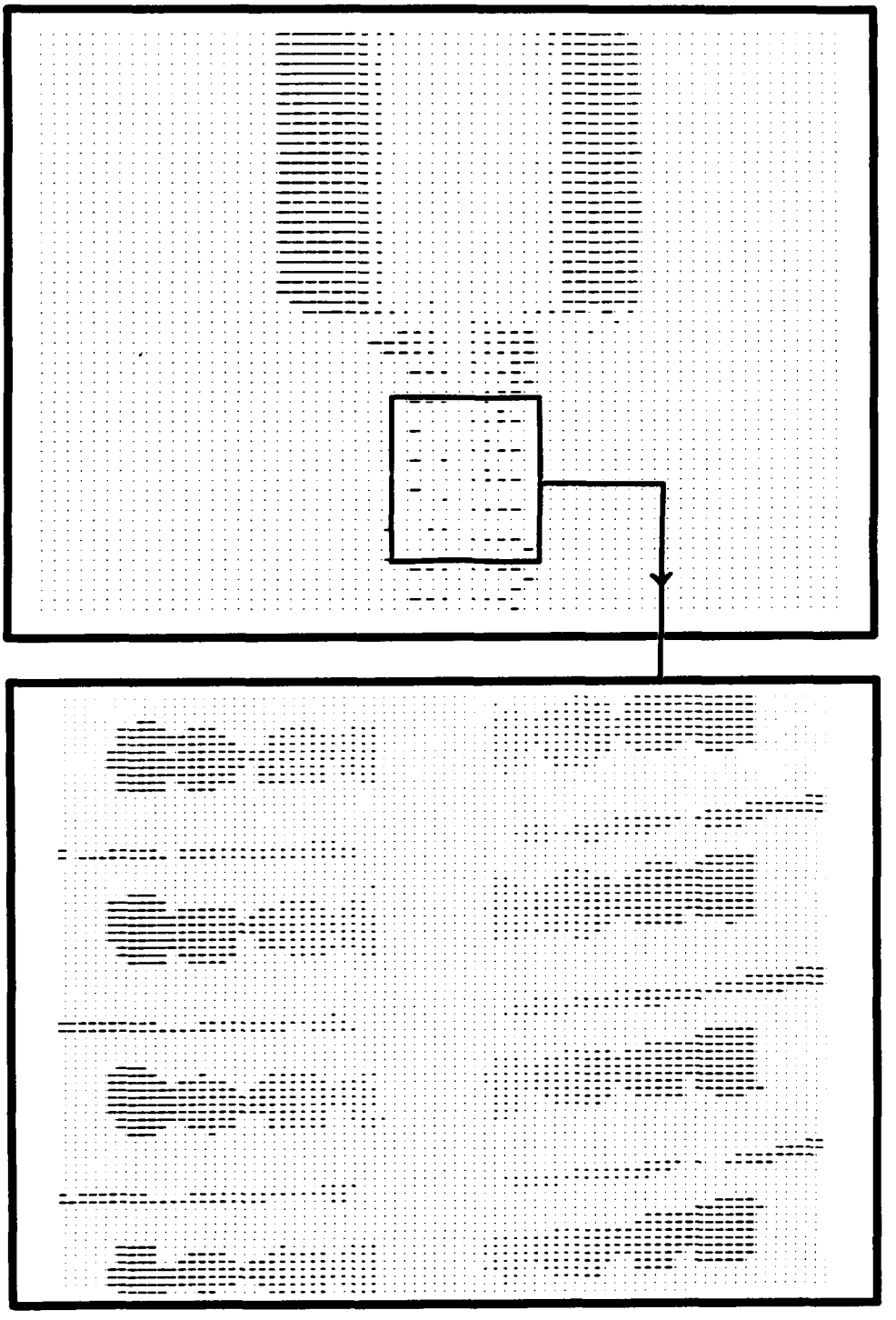

Figure 25: Needle map for the object shown in Figure 24.

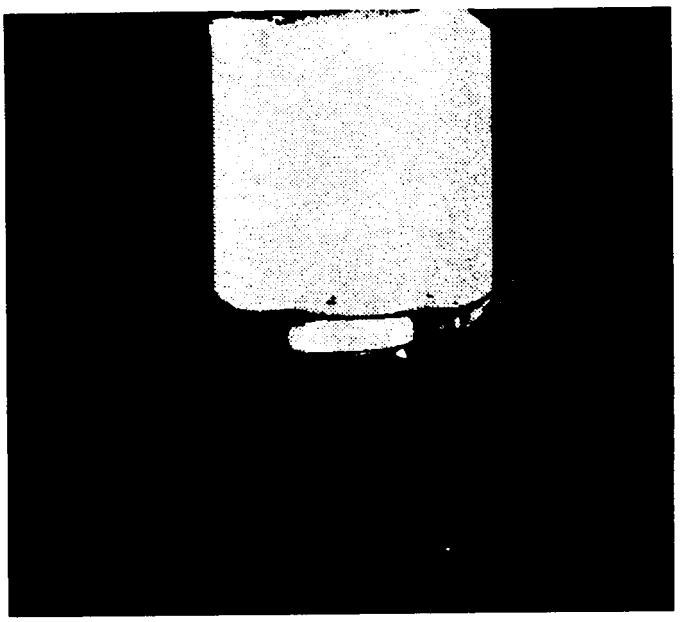

Figure 26: Lambertian strength image for the object shown in Figure 24.

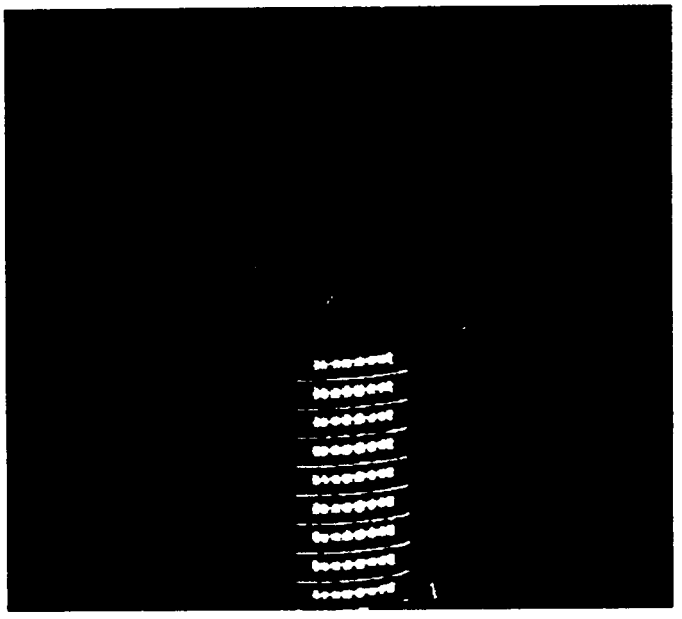

Figure 27: Specular strength image for the object shown in Figure 24.

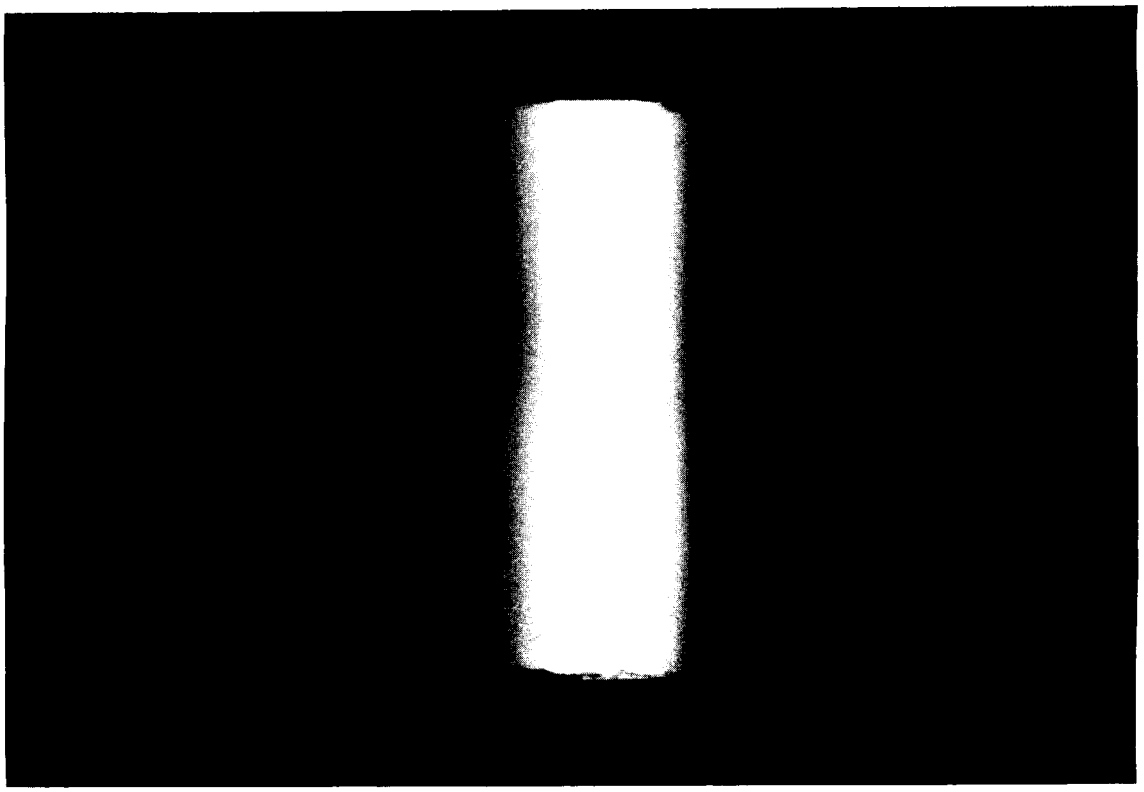

Figure 28: Photo of a cylindrical plastic object that has a hybrid surface.

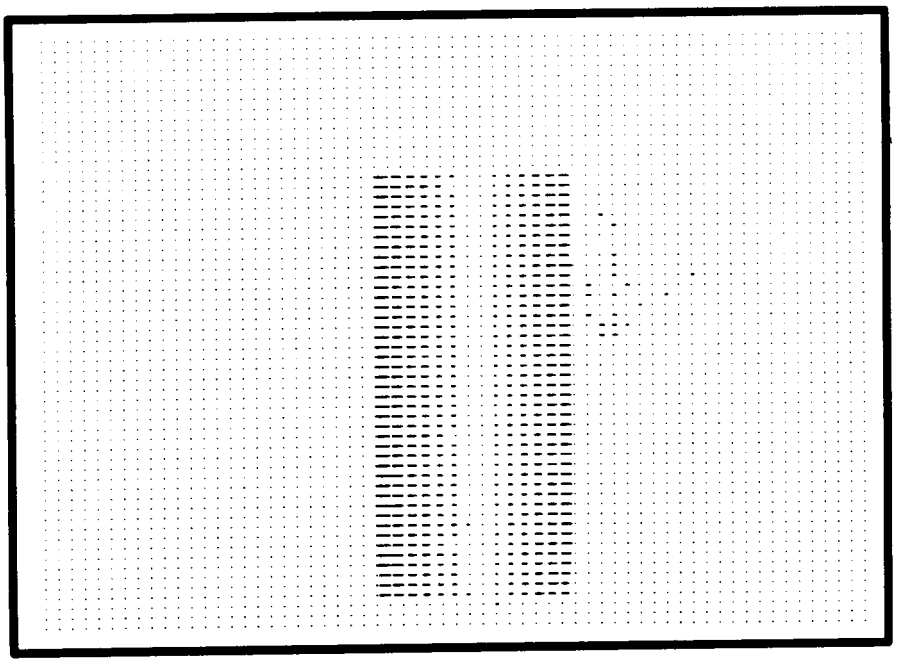

Figure 29: Needle map for the object shown in Figure 28.

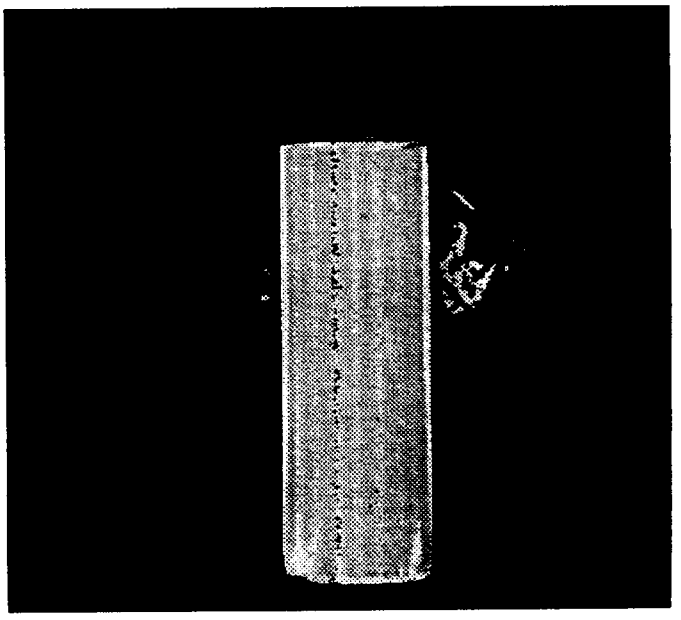

Figure 30: Lambertian strength image for the object shown in Figure 28.

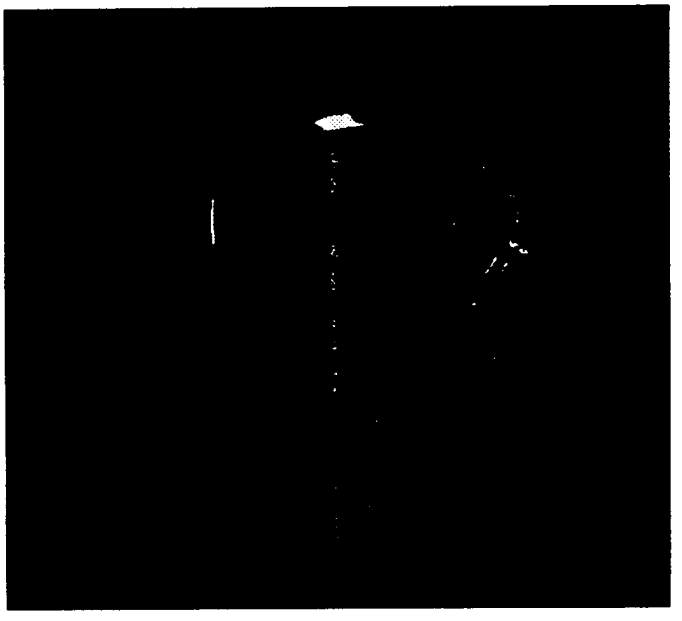

Figure 31: Specular strength image for the object shown in Figure 28.

A Generating Extended Sources

A.1 Two-Dimensional Source

An extended light source can be generated by illuminating a sheet of light-diffusing material with a point light source. Figure 32 illustrates the illumination of a section of a circular diffuser of radius R. The point source is placed at a distance H from the diffuser's surface, and the inspected object is placed at the center of the circle. The light radiance[3] $L(\theta, \theta_s)$ of the inner surface of the diffuser, due to the point source S, is proportional to the irradiance[4] $E(\theta, \theta_s)$ of the outer surface of the diffuser:

$$L(\theta, \theta_s) = CE(\theta, \theta_s). \tag{33}$$

where C is a constant of proportionality. The analytic expression for the surface irradiance $E(\theta, \theta_s)$ may be derived from the basics of radiometry as:

$$E(\theta, \theta_s) = \frac{I cos\phi}{r^2} \tag{34}$$

where I is the radiant intensity[5] of the point source S. The radiance of the extended source may be determined by expressing the variables r and ϕ in equation 34 in terms of the parameters R, H, and θ_s of the illumination geometry:

$$L(\theta, \theta_s) = \frac{CI[(R+H)cos(\theta - \theta_s) - R]}{[(R+H-Rcos(\theta - \theta_s))^2 + (Rsin(\theta - \theta_s))^2]^{3/2}}. \tag{35}$$

The radiance function $L(\theta, \theta_s)$ is symmetric, or even, with respect to $\theta = \theta_s$, and its magnitude decreases as θ deviates from θ_s. Points on the diffuser that lie in the interval θ_s-α $< \theta < \theta_s$+α receive light from the point source S. Points on the diffuser that lie outside this interval are occluded from the point source by points that lie in the interval. Thus, $L(\theta, \theta_s)$ $= 0$ for $\theta < \theta_s$-α and $\theta > \theta_s$+α. The source termination angle α may be determined from Figure 32 as:

$$\alpha = cos^{-1}\frac{R}{R+H}. \tag{36}$$

[3]Radiance is defined as the flux emitted per unit foreshortened surface area per unit solid angle. Radiance is measured in watts per square meter per steradian ($W.m^{-2}.sr^{-1}$).

[4]Irradiance is defined as the incident flux density and is measured in watts per square meter ($W.m^{-2}$).

[5]Radiant Intensity of a source is defined as the flux exiting per unit solid angle and is measured in watts per steradian ($W.sr^{-1}$).

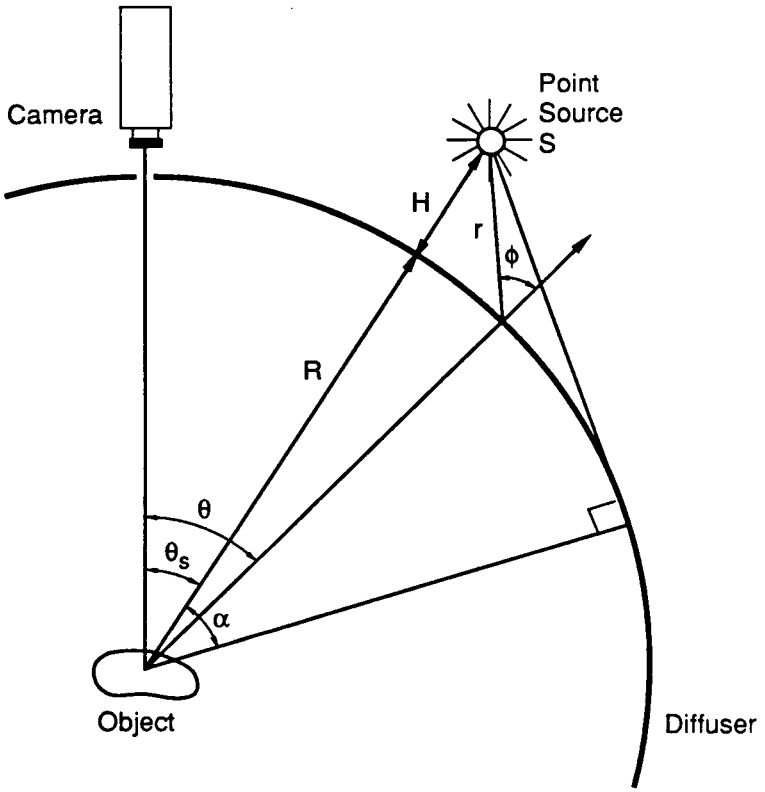

Figure 32: Two-dimensional extended source.

A.2 Three-Dimensional Source

Figure 33 illustrates the generation of a three-dimensional extended source. A spherical diffuser is illuminated with a point source of light. The radiance $L(\theta, \psi, \theta_s, \psi_s)$ of the inner surface of the diffuser, due to point source S, is determined as:

$$L(\theta, \psi, \theta_s, \psi_s) = \frac{\mathrm{CI}[(R+H)\cos\beta - R]}{[(R+H-R\cos\beta)^2 + (R\sin\beta)^2]^{3/2}}, \tag{37}$$

where:

$$\cos\beta = \cos\theta_s \cos\theta + \sin\theta_s \sin\theta \cos(\psi - \psi_s)$$

and:

$$\sin\beta = \sqrt{1 - [\cos\beta]^2}.$$

The radiance function $L(\theta, \psi, \theta_s, \psi_s)$ is symmetric about the point source direction (θ_s, ψ_s). Points on the diffuser that have equal radiance values lie on concentric circles. The magnitude

of $L(\theta, \psi, \theta_s, \psi_s)$ decreases as (θ, ψ) deviates from (θ_s, ψ_s), and $L(\theta, \psi, \theta_s, \psi_s) = 0$ for $\beta > \alpha$.

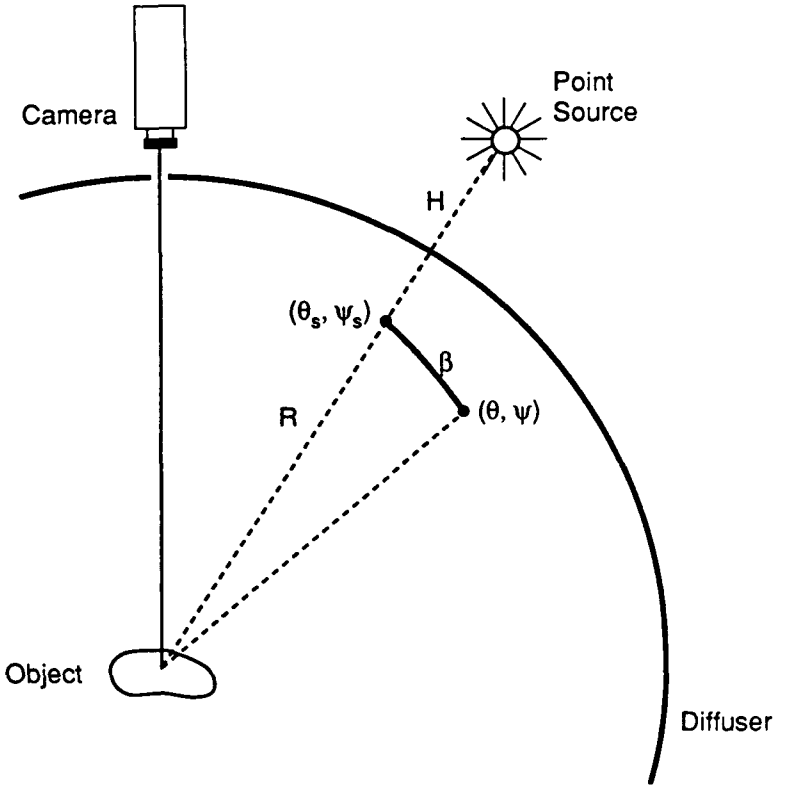

Figure 33: Three-dimensional extended source.

We have chosen a spherical diffuser since it produces symmetrical extended sources. Further, an array of extended sources is realized by simply distributing point sources around the spherical diffuser and placing the object at the center of the diffuser. All extended sources in the array would have identical radiance characteristics if all point sources have the same radiant intensity and are positioned at equal distances from the surface of the spherical diffuser.

The tessellation used to distribute the extended sources is critical from the perspective of detecting of specular reflections. A specular surface point with orientation (θ_n, ψ_n) will reflect light, from the point $(2\theta_n,\psi_n)$ on the diffuser, into the camera. As in the two-dimensional case, the location of the point $(2\theta_n,\psi_n)$ can be determined from the non-zero image intensities measured at the specular surface point. If extended sources are distributed in the icosahedron tessellation, any three adjacent point sources will constitute the vertices of an equilateral triangle. Let us assume that adjacent sources are separated by the source termination angle α.

As shown in Figure 34, the point on the diffuser that lies in the direction $(2\theta_n,\psi_n)$ can be illuminated by point sources S_k, S_{k+1}, and S_{k+2}. Therefore, for a specular surface point of orientation (θ_n,ψ_n), the image intensities I'_k, I'_{k+1}, and I'_{k+2} will be the non-zero intensities in the set $\{I'_i\}$. Since the radiance function $L(\theta, \psi, \theta_s, \psi_s)$ decreases in magnitude as we move away from the point source direction (θ_s, ψ_s), the normalized brightness difference function can be modified to help determine the point $(2\theta_n,\psi_n)$ from the three image intensities I'_k, I'_{k+1}, and I'_{k+2}.

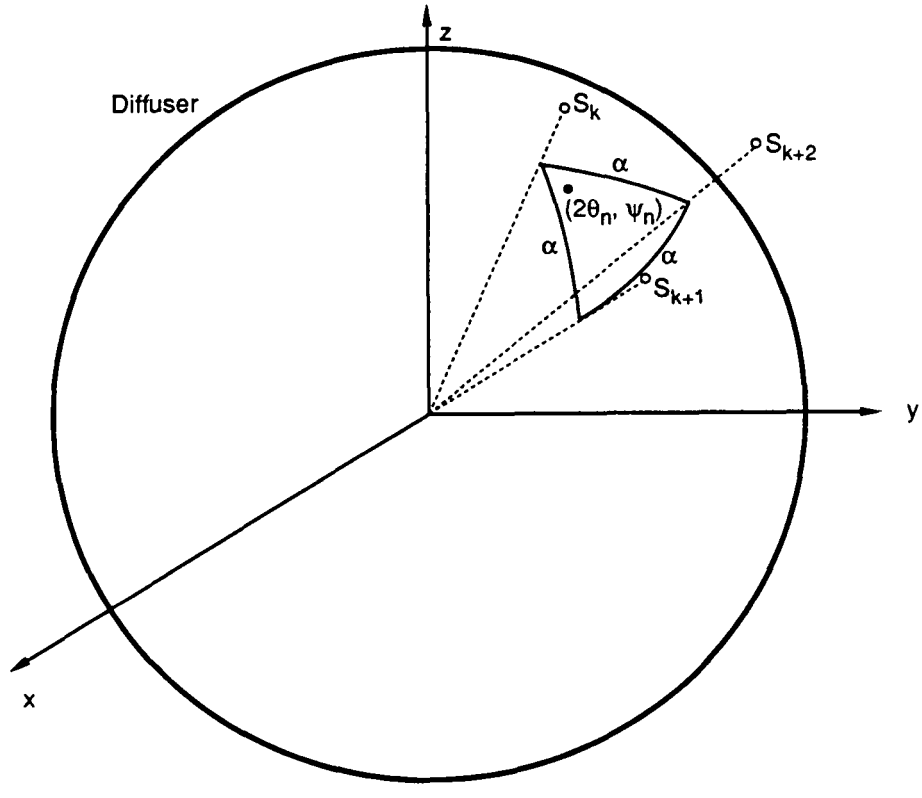

Figure 34: The point $(2\theta_n,\psi_n)$ on the surface of the diffuser lies on the extended sources generated by point sources S_k, S_{k+1}, and S_{k+2}.

Acknowledgements

The authors are grateful to Gudrun Klinker for her valuable comments and to Robert J. Stewart of Westinghouse Electric Corporation for his support and encouragement. The members of the VASC center at Carnegie Mellon University provided many useful suggestions. The authors also thank Rachel Levine, Nancy Serviou, and Ken Mohnkern for their help in preparing the manuscript.

References

[1] C. M. Brown, *Fast display of well-tessellated surfaces,* Computer and Graphics, Vol. 4, No. 2, pp. 77-85, 1979.

[2] E. N. Coleman and R. Jain, *Obtaining 3-dimensional shape of textured and specular surface using four-source photometry,* Computer Graphics and Image Processing, Vol. 18, No. 4, pp. 309-328, April, 1982.

[3] G. Healey and T. O. Binford, *Local Shape from Specularity,* Proc. Image Understanding Workshop, Vol. 2, pp. 874-887, February, 1987.

[4] B. K. P. Horn, *Shape from Shading: A Method for Obtaining the Shape of a Smooth Opaque Object from One View,* MIT Project MAC Internal Report TR-79 and MIT AI Laboratory Technical Report 232, November, 1970.

[5] B. K. P. Horn and R. W. Sjoberg, *Calculating the reflectance map,* Applied Optics, Vol. 18, No. 11, pp. 1770-1779, June 1979.

[6] B. K. P. Horn, *Image intensity understanding,* Artificial Intelligence, Vol. 8, No. 2, 1977.

[7] B. K. P. Horn, Robot Vision, MIT Press, 1986.

[8] B. K. P. Horn, *Extended Gaussian Images,* Proc. of the IEEE, Vol. 72, No. 12, pp. 1671-1686, December, 1984.

[9] K. Ikeuchi and B. K. P. Horn, *Numerical Shape from Shading and Occluding Boundaries,* Artificial Intelligence, Vol. 17, Nos. 1-3, pp. 141-184, August, 1981.

[10] K. Ikeuchi, *Numerical shape from shading and occluding contours in a single view,* Artificial Intelligence Lab., MIT, Cambridge, AI-Memo 566, 1980.

[11] K. Ikeuchi, *Determining surface orientations of specular surfaces by using the photometric stereo method,* IEEE Trans. on Pattern Analysis and Machine Intelligence, Vol. 3, No. 6, pp. 661-669, November, 1981.

[12] G. J. Klinker, S. A. Shafer, and T. Kanade, *The Measurement of Highlights in Color Images,* International Journal of Computer Vision, Vol. 2, No. 1, Spring, 1988.

[13] S. K. Nayar and A. C. Sanderson, *Determining surfaces orientations of specular surfaces by intensity encoded illumination,* Proc. SPIE, Vol. 850, pp. 122-127, November, 1987.

[14] A. P. Pentland, *Local Shading Analysis,* IEEE Trans. on Pattern Analysis and Machine Intelligence, Vol. 6, No. 2, pp. 170-187, March, 1984.

[15] B. Phong, *Illumination for Computer Generated Pictures,* Communications of ACM, Vol. 18, pp. 311-317, 1975.

[16] R. Ray, J. Birk, and R. B. Kelley, *Error Analysis of Surface Normals Determined by Radiometry,* IEEE Trans. on Pattern Analysis and Machine Intelligence, Vol. 5, No. 6, pp. 631-645, November, 1983.

[17] A. C. Sanderson, L. E. Weiss, and S. K. Nayar, *Structured Highlight Inspection of specular surfaces,* IEEE Trans. on Pattern Analysis and Machine Intelligence, Vol. 10, No. 1, pp. 44-55, January, 1988.

[18] W. M. Silver, *Determining Shape and Reflectance Using Multiple Images,* S. M. Thesis, Dept. of Electrical Engineering and Computer Science, MIT, Cambridge, Massachusetts, June, 1980.

[19] E. Sparrow and R. Cess, Radiation Heat Transfer, McGraw-Hill, 1978.

[20] K. Torrance and E. Sparrow, *Theory for Off-Specular Reflection from Roughened Surfaces,* Journal of the Optical Society of America, No. 57, pp. 1105-1114, 1967.

[21] R. J. Woodham, *Photometric stereo: A reflectance map technique for determining surface orientation from image intensity,* Proc. SPIE, Vol. 155, pp. 136-143, 1978.

[22] R. J. Woodham, *Photometric method for determining surface orientation from multiple images,* Optical Engineering, Vol. 19, No. 1, pp. 139-144, 1980.